



A National Center of Excellence in Advanced Technology Applications

ISSN 1520-295X

Low Cycle Fatigue Behavior of Longitudinal Reinforcement in Reinforced Concrete Bridge Columns

by

Jeff Brown and Sashi K. Kunnath

University of Central Florida

Department of Civil and Environmental Engineering

Orlando, Florida 32816-2450

Technical Report MCEER-00-0007

July 23, 2000

This research was conducted at the University of Central Florida and was supported by the Federal Highway Administration under contract number DTFH61-92-C-00106.

NOTICE

This report was prepared by the University of Central Florida as a result of research sponsored by the Multidisciplinary Center for Earthquake Engineering Research (MCEER) through a contract from the Federal Highway Administration. Neither MCEER, associates of MCEER, its sponsors, the University of Central Florida, nor any person acting on their behalf:

- a. makes any warranty, express or implied, with respect to the use of any information, apparatus, method, or process disclosed in this report or that such use may not infringe upon privately owned rights; or
- b. assumes any liabilities of whatsoever kind with respect to the use of, or the damage resulting from the use of, any information, apparatus, method, or process disclosed in this report.

Any opinions, findings, and conclusions or recommendations expressed in this publication are those of the author(s) and do not necessarily reflect the views of MCEER or the Federal Highway Administration.

Low-Cycle Fatigue Behavior of Longitudinal Reinforcement in Reinforced Concrete Bridge Columns

by

Jeff Brown¹ and Sashi K. Kunnath²

Publication Date: July 25, 2000
Submittal Date: August 23, 1999

Technical Report MCEER-00-0007

Task Number 106-E-5.3

FHWA Contract Number DTFH61-92-C-00106

- 1 Graduate Research Assistant, Department of Civil and Environmental Engineering, University of Central Florida
- 2 Associate Professor, Department of Civil and Environmental Engineering, University of Central Florida

MULTIDISCIPLINARY CENTER FOR EARTHQUAKE ENGINEERING RESEARCH
University at Buffalo, State University of New York
Red Jacket Quadrangle, Buffalo, NY 14261

Preface

The Multidisciplinary Center for Earthquake Engineering Research (MCEER) is a national center of excellence in advanced technology applications that is dedicated to the reduction of earthquake losses nationwide. Headquartered at the University at Buffalo, State University of New York, the Center was originally established by the National Science Foundation in 1986, as the National Center for Earthquake Engineering Research (NCEER).

Comprising a consortium of researchers from numerous disciplines and institutions throughout the United States, the Center's mission is to reduce earthquake losses through research and the application of advanced technologies that improve engineering, pre-earthquake planning and post-earthquake recovery strategies. Toward this end, the Center coordinates a nationwide program of multidisciplinary team research, education and outreach activities.

MCEER's research is conducted under the sponsorship of two major federal agencies, the National Science Foundation (NSF) and the Federal Highway Administration (FHWA), and the State of New York. Significant support is also derived from the Federal Emergency Management Agency (FEMA), other state governments, academic institutions, foreign governments and private industry.

The Center's FHWA-sponsored Highway Project develops retrofit and evaluation methodologies for existing bridges and other highway structures (including tunnels, retaining structures, slopes, culverts, and pavements), and improved seismic design criteria and procedures for bridges and other highway structures. Specifically, tasks are being conducted to:

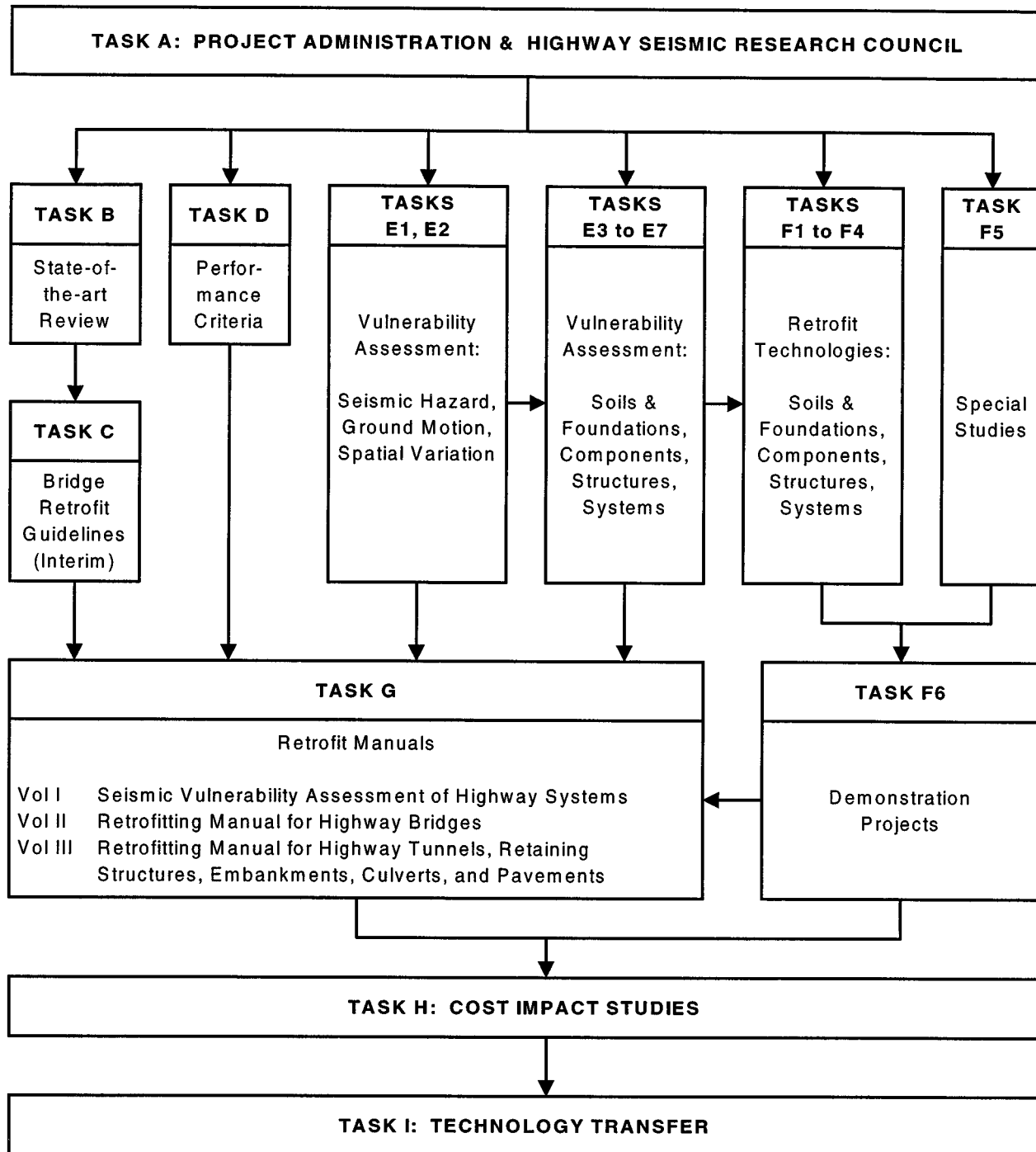
- assess the vulnerability of highway systems, structures and components;
- develop concepts for retrofitting vulnerable highway structures and components;
- develop improved design and analysis methodologies for bridges, tunnels, and retaining structures, which include consideration of soil-structure interaction mechanisms and their influence on structural response;
- review and recommend improved seismic design and performance criteria for new highway systems and structures.

Highway Project research focuses on two distinct areas: the development of improved design criteria and philosophies for new or future highway construction, and the development of improved analysis and retrofitting methodologies for existing highway systems and structures. The research discussed in this report is a result of work conducted under the existing highway structures project, and was performed within Task 106-E-5.3, "Performance-Based Specifications for the Seismic Design, Retrofit, and Repair of Reinforced Concrete Bridge Columns" of that project as shown in the flowchart on the following page.

The overall objective of this task was to develop a performance-based approach to the seismic design, retrofit and repair of reinforced concrete bridge columns, which is intended to supplement the current AASHTO design procedure. This report focuses on Phase 2 of the project, which involved using data obtained in Phase 1 to evaluate and calibrate existing analytical damage

models for reinforced concrete columns, derive improved damage models, and develop methods of using these models in practical design applications. This report describes an experimental set up for low-cycle fatigue testing of reinforcing bars, and provides an analysis of the experimental results. The study indicates that proposed fatigue-life relationships can be used in conjunction with Miner's linear damage accumulation law to identify ductile fracture and failure of reinforcing bars subjected to random strain histories resulting from seismic loading.

SEISMIC VULNERABILITY OF EXISTING HIGHWAY CONSTRUCTION
FHWA Contract DTFH61-92-C-00106



ABSTRACT

Current seismic design provisions for bridge columns rely entirely on proper detailing of potential plastic hinge zones to prevent failure of the section under repeated inelastic excursions. These provisions, however, do not offer any insight into the mechanics of damage progression and the "damaged" state of the section or component after a seismic event. Hence, the larger issue of modeling and calibrating cumulative damage resulting from a series of events, which include both elastic and inelastic cycles, remains unresolved. In a recent series of experimental tests investigating cumulative seismic damage in RC bridge piers, Kunnath et al (1997) identified low-cycle fatigue of the longitudinal reinforcing steel as one of the potential failure modes. The objective of this research is to provide an experimental database of low-cycle fatigue tests and to develop fatigue-life relationships for typical longitudinal reinforcement that aid the development of cumulative damage models.

A test setup was designed and fabricated to investigate a range of reinforcement sizes typically used as longitudinal reinforcement (#19m - #29m) in reinforced concrete bridge construction. In order to transfer a force of sufficient magnitude to induce an inelastic response in the rebar, a "swaging" concept was employed to design and fabricate a special gripping mechanism capable of resisting both tension and compression. An easily deformed material (aluminum) was securely fastened between the specimen and custom built gripping blocks. Deformation patterns present on both the specimen and grips allow for the transfer of force via shear stress through the transfer media.

In addition to constant amplitude loading needed to establish fatigue-life expressions, numerous random amplitude strain histories similar to those imposed by seismic loading were also investigated. The strain range of interest in this study was between +/- 0.015 and +/- 0.030. Existing fatigue life models based on total strain amplitude, plastic strain amplitude, and energy were applied to the recorded data from the constant amplitude experiments. These models were then used to monitor cumulative damage progression and identify failure in the random amplitude strain history experiments. Results of the study indicate that the proposed fatigue-life relationships can be used in conjunction with Miner's linear damage accumulation law to identify ductile fracture and failure of reinforcing bars subjected to random strain histories resulting from seismic loading.

It was determined that bar size has a small but noticeable effect on fatigue life. Reinforcing bars with larger diameters exhibited improved fatigue characteristics. Better correlations were obtained with damage models using total strain and plastic strain as opposed to energy-based formulations. The rate of strength (stress) decay across tension peaks of the rebar can be an important precursor of failure. Strength loss beyond 75% of the original peak stress was rapid and catastrophic. The rate of decay for compression cycles was masked by local buckling phenomena. The rainflow counting method was found to be satisfactory in dealing with random strain amplitudes, as would be expected in earthquake loading.

ACKNOWLEDGMENTS

Financial support for this project was provided through the Multidisciplinary Center for Earthquake Engineering Research (MCEER) and the National Institute of Standards and Technology (NIST).

The experimental work reported herein was conducted at the Structural Testing Laboratory at NIST by Jeff Brown as part of his Master's thesis at the University of Central Florida. The following individuals at NIST provided invaluable input to the experimental planning and design: H.S. Lew, Nick Carino, Bill Stone and Mike Riley. Finally, special thanks are due to the technical staff in the Structural Testing Laboratory at NIST: Steve Johnson, Frank Davis, Max Peltz and Erik Anderson - whose assistance was instrumental in the successful completion of the rebar fatigue experiments.

TABLE OF CONTENTS

SECTION	TITLE	PAGE
1.0	INTRODUCTION.....	1
1.1	Background	2
1.2	Research Objectives and Scope of Study	3
1.3	Organization of Report.....	4
2.0	EVALUATION OF SELECTED DAMAGE MODELS.....	5
2.1	Fatigue-Based Damage Models.....	5
2.2	Selected Control Damage Models.....	7
2.3	Calibration of Damage Models	9
2.4	Performance of Selected Damage Models.....	14
2.4.1	Standard Cyclic Loading.....	14
2.4.2	Constant Amplitude Loading	16
2.5	Summary	16
3.0	DESIGN OF EXPERIMENTAL SETUP FOR LOW-CYCLE FATIGUE TESTING OF REINFORCING BARS	23
3.1	Background	23
3.2	Review of Literature.....	24
3.2.1	The Fatigue Process.....	24
3.2.2	High Cycle Fatigue in Concrete Reinforcement	26
3.2.3	Low-cycle Fatigue in Concrete Reinforcement.....	26
3.3	Test Setup	30
3.3.1	Hydraulic Actuator and Reaction Frame.....	31
3.3.2	Force Transfer to Specimen.....	33
3.3.3	Prototype Rebar Grip.....	36
3.3.4	Load and Deformation Measurements	37
3.3.5	Data Acquisition and Control.....	39
3.4	Summary	40
4.0	RESULTS OF FATIGUE TESTS ON REINFORCING BARS.....	41
4.1	Constant Amplitude Testing.....	41
4.1.1	Specimen Preparation.....	41
4.1.2	Observations and Results	42
	<u>#19m Specimens</u>	45
	<u>#22m Specimens</u>	47
	<u>#25m Specimens</u>	49

TABLE OF CONTENTS (CONT'D)

SECTION	TITLE	PAGE
4.2	Random Amplitude Testing	51
4.2.1	Generation of Random Amplitude Strain Histories	51
4.3	Observations	56
4.4	Summary	59
5.0	ANALYSIS OF EXPERIMENTAL RESULTS.....	61
5.1	Fatigue-life Models.....	61
5.1.1	Total Strain Amplitude	62
5.1.2	Plastic Strain Amplitude	64
5.1.3	Energy Based Formulations.....	69
5.2	Observations on Stress vs. Strain Behavior	70
5.3	Random Amplitude Strain History Analysis	73
5.3.1	Rainflow Cycle Counting Method.....	73
5.3.2	Calculated Damage Indices.....	74
5.4	Cumulative Damage Approach.....	77
5.5	Application to Reinforced Concrete	80
5.6	Comparison With Previous Work (Mander et al, 1994).....	81
5.7	Summary	83
6.0	REFERENCES	85

LIST OF FIGURES

FIGURE	TITLE	PAGE
2-1	Effect of Variations in Plastic Hinge Length on Cumulative Damage	11
2-2	Effect of Varying Model Constants on Damage Prediction.....	12
2-3	Cumulative Damage to Circular Columns, Standard Cyclic Loading, Selected Damage Models	17
2-4	Cumulative Damage to Circular Columns, Constant Amplitude Loading, $2\delta_y$, Selected Damage Models	18
2-5	Cumulative Damage to Circular Columns, Constant Amplitude Loading, $2\delta_y$, Selected Damage Models	19
2-6	Cumulative Damage to Circular Columns, Constant Amplitude Loading, $4\delta_y$, Selected Damage Models	20
2-7	Cumulative Damage to Circular Columns, Constant Amplitude Loading, $5\delta_y$, Selected Damage Models	21
3-1	Typical Fatigue-life Curve for an Engineering Alloy	25
3-2	Slipband Extrusion and Initial Crack Formation (Smith, 1990)	25
3-3	(a) Gage length of rebar specimen used in present testing (b) Typical fatigue test specimen used in conventional testing	32
3-4	Actuator and box beams anchored to strong floor.....	32
3-5	General schematic of load frame and hydraulic actuator (dimensions in cm)	33
3-6	Force transfer to specimen gage length.....	34
3-7	Assumed shear stress distribution within development length	35
3-8	Detail drawing of pilot grip for use with Grade 60, #16 rebar	36
3-9	Detail drawing of prototype grip (all units in cm).....	37
3-10	Prototype rebar grip.....	38
3-11	Load cell with actuator and grip adapters.....	38
3-12	LVDTs and extensometer used for deformation measurements	39
3-13	Schematic of closed loop hydraulic control	40
4-1	Force Transfer Media Detail	41
4-2	Deformation of Force Transfer Media with UTM.....	42
4-3	Specimen in Grips Ready for Bolting	43
4-4	Securing Specimen in Rebar Grip	43
4-5	Completed Specimen Ready for Testing.....	44
4-6	Stress vs. Strain data: Experiment #24.....	44
4-7	Location of Fatigue Crack Formation	45
4-8	Fatigue-life Data (total strain)	46
4-9	Fatigue-life Data (Plastic Strain).....	46
4-10	Strain Amplitude vs. Total Energy to Failure	47
4-11	Fatigue-life Data (Total Strain)	48
4-12	Fatigue-life Data (Plastic Strain).....	48

LIST OF FIGURES (CONT'D)

FIGURE	TITLE	PAGE
4-13	Strain Amplitude vs. Total Energy to Failure	49
4-14	Fatigue-life Data (Total Strain)	50
4-15	Fatigue-life Data (Plastic Strain).....	50
4-16	Strain Amplitude vs. Total Energy to Failure	51
4-17	Assumed Curvature-Strain Relationship	53
4-18	Stress vs. Strain Data: Experiment #48	57
4-19	Fatigue Crack Just Prior to Failure (Experiment #48).....	58
4-20	Final State of Specimen After Rupture	58
5-1	Simple Constant Amplitude Strain History	62
5-2	Fatigue-life Curves Considering Total Strain Amplitude	64
5-3	Fatigue-life Curves Modified for Max Stress at Specimen Half-Life	65
5-4	Plastic Strain Amplitude, $\Delta\epsilon_p$	66
5-5	Fatigue-life Curves Considering Plastic Strain Amplitude	67
5-6	Plastic Strain FLCs Modified for Max Stress at Specimen Half-Life.....	68
5-7	Total Strain Amplitude vs. Energy to Failure	70
5-8	f_i/f_o vs. Nf for Different Strain Amplitudes (Tension Peaks).....	72
5-9	f_i/f_o vs. Nf for Different Strain Amplitudes (Compression Peaks)	72
5-10	Sample random load history to demonstrate rainfall counting method.....	75
5-11	Cumulative Damage in Generic Constant Amplitude Experiment	79
5-12	Cumulative Damage in Experiment #41	79
5-13	Damage Progression and Resulting Potential Failure Modes	81
5-14	Comparison of Fatigue-life Curves: Current Study and Mander et al (1994).....	82

LIST OF TABLES

Table	TITLE	PAGE
2-1	Hysteresis Parameter Assignments, Flexural Column	9
2-2	Summary of Bridge Column Tests Considered in Evaluation	15
2-3	Peak Cumulative Damage for Circular Columns Subjected to Standard Cyclic Loading, Selected Damage Models	17
2-4	Peak Cumulative Damage for Circular Columns Subjected to Constant Amplitude Cyclic Loading, $2\delta_y$, Selected Damage Models	18
2-5	Cumulative Damage for Circular Columns Subjected to Constant Amplitude Cyclic Loading, $3\delta_y$, Selected Damage Models	19
2-6	Peak Cumulative Damage for Circular Columns Subjected to Constant Amplitude Cyclic Loading, $4\delta_y$, Selected Damage Models	20
2-7	Peak Cumulative Damage for Circular Columns Subjected to Constant Amplitude Cyclic Loading, $5\delta_y$, Selected Damage Models	21
3-1	Fatigue-life Model Curve Fits (Mander et al, 1994)	29
3-2	Mill Report Data for Rebar Specimens	31
4-1	#19m Specimens: Constant Amplitude Results	45
4-2	#22m Specimens: Constant Amplitude Results	47
4-3	#25m Specimens: Constant Amplitude Results	49
4-4	Description of Load History Classes Used for Random Testing	52
4-5	Imposed Strain Histories for Random Amplitude Experiments.....	54
5-1	Summary of Fatigue-life Curves: Koh and Stephens' Model for Total Strain	65
5-2	Summary of Fatigue-life Curves: Koh and Stephens' Modified for Strength	66
5-3	Summary of Fatigue-life Curves: Coffin-Manson Model for Plastic Strain	66
5-4	Summary of Fatigue-life Curves: Lorenzo and Laird Modified for Strength	67
5-5	Curve Fit Data for Energy Based Models Proposed by Mander et al (1994).....	70
5-6	Resulting Deformation Ranges from Sample Strain History	75
5-7	Calculated Damage Indices for Random Amplitude Experiments.....	78
5-8	Fatigue-life Summary (Curve Fit Predictions).....	83

SECTION 1

INTRODUCTION

This project is a continuation of a previous research effort sponsored by the Federal Highway Administration, the Multidisciplinary Center for Earthquake Engineering Research (then National Center for Earthquake Engineering Research), the California Department of Transportation and the National Institute of Standards and Technology. The primary scope of the previous project was to examine progressive damage in reinforced concrete bridge piers. The eventual goal of the research is to contribute to current efforts in the development of performance-based criteria for the seismic design, retrofit, and repair of reinforced concrete bridge columns.

Phase I of the project focused on the experimental behavior of typical CALTRANS circular columns subjected to fatigue and random loading. At the end of phase I, twelve quarter scale bridge columns were tested to failure under monotonic, low-cycle fatigue and analytically simulated random amplitude loading. The objectives of Phase II of the project was to utilize the experimental data obtained in Phase I and to evaluate and calibrate existing analytical damage models for reinforced concrete bridge columns. Further, the study was also concerned with deriving fundamental relations to improve existing damage model formulation so as to enable their use in practical design applications.

In the first part of the Phase II project, a comprehensive review of existing damage models was carried out so as to arrive at a set of typical models for subsequent evaluation and validation against observed test data. Initial findings from the analytical study indicate that the damage is controlled primarily by the inelastic low-cycle fatigue behavior of the main longitudinal reinforcement and the strain energy capacity of transverse hoop reinforcement.

It was, therefore, concluded that a more detailed understanding of the low-cycle fatigue behavior of reinforcing bars was essential to the development of a predictive damage model for bridge columns. Much of the remaining effort in Phase II concentrated on developing fatigue

relationships for reinforcing bars under the action of constant-amplitude (strain) loading and assessing the suitability of such fatigue-life expressions for predicting the cumulative damage under random amplitude loading.

Details of the various tasks undertaken during the Phase II effort are summarized in this report.

1.1 Background

Current seismic design provisions rely entirely on proper detailing of potential plastic hinge zones to prevent failure of the section under repeated inelastic excursions. These provisions, however, do not offer any insight into the mechanics of damage progression and the "damaged" state of the section or component after a seismic event. Hence, the larger issue of cumulative damage, resulting from a series of events that include both elastic and inelastic cycles, remains unresolved.

As more research results on the non-linear response of RC structures in general, and RC bridge columns in particular, become available, a performance based design approach that addresses the relationship between structural response and damage limit states is becoming more feasible. If the seismic demands in a structural component (and thereby, the entire structure) can be estimated, and a structure then designed to withstand the entire deformation history expected throughout its service life, structural failure due to accumulated seismic damage may be controlled with greater reliability.

Based on the evaluation of numerous experimental tests on RC components and sub-assemblies, the following three failure modes have been identified as potential causes for the loss of ductility and/or energy-dissipation capacity of RC members (Mander and Cheng, 1995):

1. Low-cycle fatigue of the longitudinal reinforcing steel
2. Failure of core concrete due to lack of confinement or fracture of transverse reinforcement

3. Compression buckling of the longitudinal reinforcement

The above modes are exclusively flexural failure modes and modes 2 and 3 are not necessarily independent of each other. The subject of shear failure is a separate and critical issue but not the subject of this study. Hence, any failure mode leading to brittle shear failure is not addressed.

If proper detailing methods (such as the provision of closely spaced transverse reinforcement) are employed in plastic hinge regions, failure modes two and three listed above can be avoided. Hence, it can be stated that low-cycle fatigue failure of longitudinal reinforcement is the final unavoidable failure mode. Low-cycle fatigue is defined as failure in a material due to a relatively small number of load or deformation cycles (< 1000) and typically involves large deformations that exceed the elastic limit. With the exception of a small series of tests conducted at SUNY Buffalo (Mander et al, 1994), very little data exists on the low cycle fatigue behavior of steel reinforcement used in reinforced concrete construction.

The current research attempts to provide new experimental data on the low-cycle fatigue behavior of reinforcing bars used in concrete construction. Isolating the reinforcement and examining its behavior outside the context of a RC column may appear to be a gross simplification of correlating seismic damage in reinforced concrete members. However, for advanced analytical models that use constituent material behavior as the basis for global modeling, this information will be vital in inelastic structural response prediction and damage assessment following a seismic event. Considering the high cost associated with full scale seismic testing, the development of such models can play a significant role in damage prediction.

1.2 Research Objectives and Scope of Study

The overall scope of the research effort is to investigate cumulative seismic damage in RC bridge piers. The first phase of the study examined the response of twelve quarter-scale model bridge columns to constant amplitude and random cyclic displacement amplitudes. The conclusion from that investigation which is most relevant to the present study was that damage progression

in flexural elements is closely related to the performance of the longitudinal reinforcing steel and that a comprehensive experimental study investigating its low-cycle fatigue behavior under random cyclic loading is needed (Kunnath et al, 1997). The following tasks were carried out to accomplish the project objectives:

- Design and implementation of an experimental setup to investigate the low-cycle fatigue behavior of steel reinforcing bars. The setup should accommodate bar sizes typically used as longitudinal reinforcement in RC bridge piers.
- Examine methods for measuring equivalent longitudinal strains in reinforcing bars using member rotations or end displacements since these are readily established in analytical evaluations using nonlinear computer software.
- Apply existing fatigue-life models to the observed data for comparison with results of previous experiments conducted by other investigators.
- Investigate load path effects (randomness) on damage progression.
- Develop fatigue-life relationships for typical reinforcing bars.

1.3 Organization of Report

This report is organized in five sections. Section 2 describes the preliminary work that was conducted to analyze experimental data generated in Phase I research and other available experimental data from previous testing carried out at NIST. The evaluation of selected damage models in terms of their ability to track progressive damage is the focus of Section 2. Details of the experimental setup and general issues regarding inelastic testing procedures of reinforcing bars is outlined in Section 3. In Section 4, experimental results from constant amplitude tests and variable amplitude (simulated seismic loading) tests are presented. A systematic evaluation of the observed results and the application of fatigue-life models to the recorded data are presented in Section 5. Significant findings from the present study and recommendations for future work are also discussed in Section 5.

SECTION 2

EVALUATION OF SELECTED DAMAGE MODELS

2.1 Fatigue-Based Damage Models

A few fatigue-based models and some control damage models were evaluated in this phase of the study. Low-cycle fatigue theory is a topic that was originated and advanced for steel construction many years ago. Only more recently has this discussion been extended to reinforced concrete. Coffin (1954) and Manson (1953) were among the first to propose an equation relating strain amplitude to the number of cycles to failure:

$$\varepsilon_p = \varepsilon'_f (2N_f)^c \quad (2-1)$$

where:

ε_p = plastic strain amplitude

ε'_f = a material constant to be determined from fatigue testing

$2N_f$ = number of complete cycles to failure

c = fatigue exponent

Kunnath et al. (1997) calibrated the model coefficients ε'_f and c to RC specimens as composite sections. The constants defined below were derived from an experimental curve fit of the data obtained from extensive testing of the quarter-scale flexural columns subjected to constant amplitude cyclic loading:

$$\varepsilon_p = 0.074 (2N_f)^{-0.50} \quad (2-2)$$

$$\varepsilon_a = 0.070 (2N_f)^{-0.45} \quad (2-3)$$

where:

ε_a = total strain amplitude

The above refined $\varepsilon - 2N_f$ relationships were used to develop a new cumulative damage model for flexural fatigue of RC bridge piers, one of three fatigue-based models considered for further evaluation in this report. Cumulative damage is computed from:

$$D = \sum \frac{1}{2N_f} \quad (2-4a)$$

$$2N_f = \left(\frac{\varepsilon_p}{0.074} \right)^{-2.0} \quad (2-4b)$$

Note that Equation 4a and 4b defines the $\varepsilon - 2N_f$ relationship in terms of plastic rather than total strain amplitude.

The second fatigue-based model considered is the cumulative damage model proposed by Wang and Shah (1987) based on the maximum deformation occurring in a cycle:

$$D = \frac{e^{\eta B} - 1}{e^{\eta} - 1} \quad (2-5)$$

where:

$$B = c \cdot \sum_i \frac{\delta_{m,i}}{\delta_f} \quad (2-5b)$$

c and η are again user-defined constants with c based purely on experimental testing and η dependent on the span-to-depth ratio and the amount of shear reinforcement.

Each of the two models considered so far are based exclusively on low-cycle fatigue theory in that only damage associated directly with yield and fracture of the longitudinal reinforcement is considered. A second relevant failure mode relating to confinement failure (failure of the hoop reinforcement) exists and may in fact be dominant under certain types of inelastic cycling loading. Modeling damage associated with confinement failure is somewhat more complex and was not represented in either of the first two models considered.

McCabe and Hall (1994) have proposed a unique structural damage model with similarities to energy-based models but with a unique means of normalization whereby the hysteretic energy corresponding to complete damage, H_t , is a function of measured hysteretic ductility and the number of cycles to failure (which are each in turn functions of maximum attained strain for each hysteresis cycle). H_p and H_n refer to the positive and negative contributions.

$$DI = \left[\frac{H_p + H_n}{H_t} \right]^2 + \left[\frac{H_p - H_n}{H_t} \right]^2 \quad (2-6)$$

$$H_t = \mu^* P_y \delta_y (2N_f) \quad (2-6b)$$

$$\mu^* = \mu_p \cdot (2N_f)^{-\gamma} \quad (2-6c)$$

P_y and δ_y represent the familiar member yield strength and displacement, respectively. μ^* and μ_p are the hysteretic and monotonic plastic ductility, respectively. γ is a calibration constant, proposed equal to -0.6 for steel, but currently undefined for RC elements. The damage models referred to in Equations 2-4 through 2-6 will henceforth be referred to as Fatigue-1, Fatigue-2 and Fatigue-3, respectively.

2.2 Selected Control Damage Models

To characterize and contrast results obtained from Fatigue-1 through Fatigue-3, three other well known indices have been chosen for further analysis. Park and Ang's hybrid model (defined throughout as "Hybrid") combines measures of ductility and dissipated hysteretic energy to predict cumulative damage.

$$D = \frac{\delta_m}{\delta_u} + \beta \frac{\int dE}{P_y \delta_u} \quad (2-7)$$

where: δ_m = maximum deformation experienced by element

δ_u = ultimate deformation capacity of the element

β = a user-defined control parameter that control the rate of strength degradation

dE = dissipated energy by the element

P_y = yield strength of the element

Note that the denominator in the second term of Equation (2-7) is a normalizing factor which should have the same units as the energy term in the numerator.

Kratzig et al. (1987) postulated a damage model which concerns itself purely with dissipated hysteretic energy, differentiating only between what is termed primary and follower dissipated energy. The “Energy” model is expressed as:

$$D_Q^+ = \frac{\sum E_{si}^+ + \sum E_i^+}{E_u^+ + \sum E_i^+} ; \quad D_Q^- = \frac{\sum E_{si}^- + \sum E_i^-}{E_u^- + \sum E_i^-} \quad (2-8)$$

where: D_Q = damage index

E_{si} = Energy dissipated in primary cycle

E_i = Energy dissipated in follower cycle

E_u = Energy at ultimate deformation

In the above expression, the positive and negative superscripts refer to the energy dissipated in the positive and negative cycles of loading.

And finally, a modified form of the damage index proposed by Lybas and Sozen (1977), based on the principle of softening or stiffness degradation, is evaluated. This “Softneing Index” presented in Equation 2-9 is used to enable the description of a normalized quantity which does not exceed unity:

$$D_r = 1 - \frac{k_r}{k_0} \quad (2-9)$$

where: D_r = Damage index

k_r = Reduced secant stiffness at maximum deformation

k_o = Initial stiffness

2.3 Calibration of Damage Models

In order to carry out a reliable evaluation, it was necessary to calibrate the models using some baseline data. Additionally, since all inelastic evaluations were conducted using the IDARC (Kunnath et al., 1992) computer program, it was also necessary to calibrate the hysteretic parameters to be used in all evaluations. Only flexural response is considered in these evaluations.

Stone and Cheok (1989) performed the first laboratory testing of full-scale reinforced concrete circular bridge piers. Two full-scale columns were fabricated, the first a flexural member with an aspect ratio of 6 and the second, a shear column with an aspect ratio of 3. Each was subjected to quasi-static cyclic loading to failure. Available experimental data was used to calibrate the hysteresis parameters. For this test, referred to here as test Case A1, the member was subjected to a standardized quasi-static cyclic loading regimen until failure. The hysteresis parameter data set for flexural columns is provided in Table 2-1.

Table 2-1 Hysteresis Parameter Assignments, Flexural Column

	HC	HS	HBD	HBE
Flexural Member	4.0	1.0	0.0	0.1

Each of the three fatigue damage models is a function of one or more parameters. Some of these such as member yield strength or plastic hinge length are physical system properties. Others, like γ in the McCabe or ε in Wang-Shah are calibration constants that must be addressed based

on experimental test data. Ideally, a robust model will demonstrate relative insensitivity to variations in the fixed parameters on which it is based.

Consider first plastic hinge length, l_p , a parameter which affects the Fatigue-1 and Fatigue-3 models. Plastic hinges are localized regions within an element which deform plastically when element yield strength is exceeded. In circular reinforced concrete columns subjected to lateral loading, a plastic hinge will typically develop at approximately $0.75D$ from the base of the column where D is defined as column diameter. Assuming that plastic rotation takes place about the center of the plastic hinge (at height l_p), plastic curvature, Φ_p , can be defined in terms of l_p as follows (Paulay and Priestley, 1992):

$$\Phi_p = \frac{\theta_p}{l_p} = \frac{\Delta_p \div (L - 0.5l_p)}{l_p} \quad (2-10)$$

The above expression provides an approximate estimate of the average curvature and is not to be considered a measure of the maximum plastic curvature. Assuming plane-section theory, the relationship between plastic strain index, ε_p and plastic curvature can then be applied. In the equation below, \bar{d} is the depth of the section measured between centers of longitudinal bars.

$$\varepsilon_p = \Phi_p \bar{d} / 2 \quad (2-11)$$

Fatigue-1 demonstrated less sensitivity than Fatigue-3 to variations in plastic hinge length, indicating that Fatigue-3 is more sensitive to small variations in plastic strain amplitude, which is also a function of the post-yield stiffness. $l_p = 0.8D$ provided the best results (calibrated to experimental tests) for each of the models that used plastic-hinge length as a variable. Figure 2-1 shows the performance of the Fatigue-1 model to variations in plastic hinge length.

In addition to relying on one or more physical parameters, a number of the models rely on control parameters or weighting factors which must be calibrated with respect to experimental data. The Fatigue-2 damage model is calibrated using two constants, c and η . Fatigue-3 is

defined with the aid of a calibration constant, γ . Park and Ang also includes a control parameter, β , on the second term of their damage index to limit damage associated with normalized energy absorption. Figure 2-2 provides calibration data on each of these constants.

The Fatigue-2 model proposed by Wang and Shah proved most difficult of the three fatigue-based models to calibrate. The authors used data from destructive testing of a 1:4 scale beam-column joint subjected to a cyclic loading regimen to calibrate their model; geometry substantially different from the circular columns (flexural and shear) considered in this discussion.

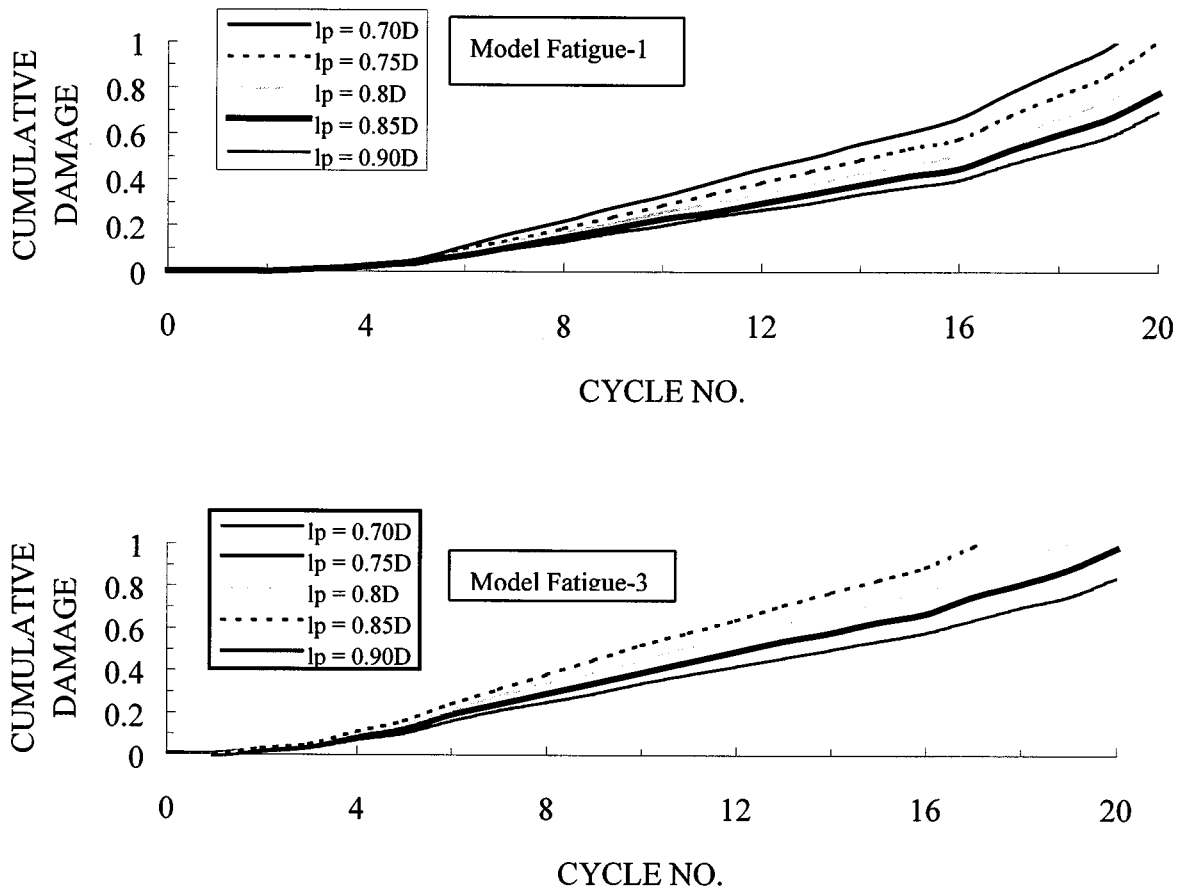


Figure 2-1 Effect of Variations in Plastic Hinge Length on Cumulative Damage

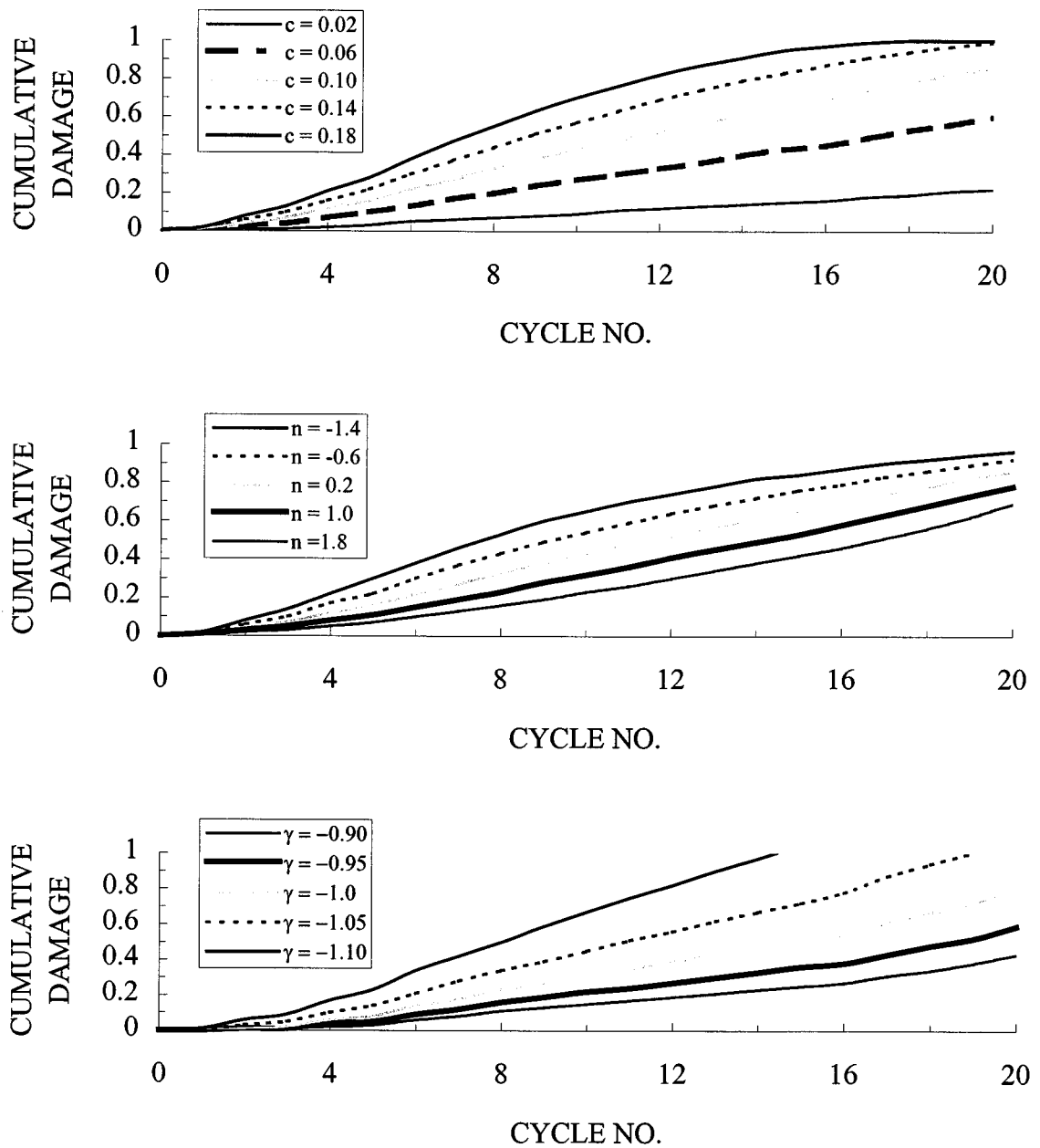


Figure 2-2 Effect of Varying Model Constants on Damage Prediction

(Note: c & n refer to c & η in Equation 2-5 and γ refers to Equation 2-6c)

In this study, effort centered on calibrating the model with respect to the flexural column. Wang and Shah propose a value of $c = 0.1$ for the first calibration constant. Values from 0.02 to 0.18 were attempted with η , the second control parameter, set to its baseline value of $\eta = 1.0$. Widely

diverging results were obtained with $c = 0.1$, in fact, yielding the best solution. Varying η affected the damage gradient, or relative change in damage with respect to the previously computed value, more so than the final result as damage in each case attempts to converge to unity. The damage progression for $\eta > 0$ reflects an increasing damage gradient, where a more gradual progression of damage is evident initially, consistent with observed results. Conversely, $\eta < 0$ returns curves that could be described as more convex in nature indicating more rapid damage accumulation early and during intermediate cycling. Values of η just greater than zero provide results that best reflect experimental data yielding both a sufficiently gradual damage progression with an adequate ultimate result. η was set equal to 0.2 for all cases.

Fatigue-3, proposed by McCabe et al. also proved highly sensitive to, γ , the model's calibration constant. Recall, γ is used to equate monotonic plastic ductility, μ_p , to what is termed hysteretic plastic ductility, μ^* . The author defines μ^* as the level of plastic ductility that results in equivalent damage over a given number of cycles as that which would occur by monotonically loading the member to plastic ductility μ_p . The relationship restated:

$$\mu^* = \mu_p \cdot (2N_f)^{\gamma} \quad (2-12)$$

McCabe et al. suggest $\gamma = -0.6$ be specified for steel. Here, values from -0.90 to -1.10 banded the acceptable range of damage output for the RC columns considered. Considerable variability exists in the rate of damage progression over that range with $\gamma = -1.05$ yielding the best result. On a more positive note, the same value of γ appears useful for evaluating both flexural and shear columns, a substantial consideration.

The Park-Ang hybrid damage model uses a weighting function, β , to limit the damage contribution attributed to dissipated hysteretic energy. The author suggests it is a function of confinement ratio, ρ_w , shear span ratio, l/d , longitudinal steel ratio, p_t , and axial stress, n_o and can be derived from the following expression (Park et al, 1987):

$$\beta = \left(-0.447 + 0.073 \frac{l}{d} + 0.24n_o + 0.314p_t \right) \times 0.7^{\rho_w} \quad (2-13)$$

where:

$$l/d = 1.7 \text{ if } l/d < 1.7$$

$$n_o = 0.2 \text{ if } n_o < 0.2$$

$$p_t = 0.75\% \text{ if } p_t < 0.75\%$$

(longitudinal steel ratio is expressed as a percentage)

Kunnath et al. (1992) list the strength degrading hysteresis parameter, β , as a user-defined parameter in IDARC. This value was assigned as part of the calibration process and is defined in Table 2.1 as HBE.

2.4 Performance of Selected Damage Models

The calibrated models selected for evaluation will now be analyzed with respect to selected laboratory testing performed at the National Institute of Standards and Technology (NIST). Test data selected include: a full-scale flexural test on a bridge column subjected to standard cyclic loading to failure; analytically simulated constant amplitude tests on the same full-scale specimen; constant amplitude tests of quarter-scale specimens tested by Kunnath et al. (1997); and finally, random amplitude testing also carried out by Kunnath et al. (1997). In the tests conducted by Kunnath and El-Bahy, variability was limited to loading type (amplitude and sequence) thus providing an excellent subset of data to validate the damage models. The test data utilized in the evaluation study is summarized in Table 2-2.

2.4.1 Standard Cyclic Loading

Cumulative damage progression versus number of cycles is shown in Figure 2-3 for each of the models considered. Peak damage indices are provided in Table 2-3. Predictably, the Softening Index indicates the most rapid damage progression, with damage near unity indicated after just six cycles. The Energy model proposed by Kratzig also displays significant damage early, incompatible with the observed result. The Park model, based on a combination of ductility and

energy measures, shows a more gradual damage progression, somewhat linear in nature. This type of progression is closer to what might be observed experimentally, but again, indicated damage is over-stated initially and through the mid-portion of the test.

Table 2-2 Summary of Bridge Column Tests Considered in Evaluation

Column Description	Case	L (length)	D (dia.)	δ_y (yield disp)	P_y (yield strength)	Peak Drift (%)	$2N_f$	Excitation Type
Full Scale Flexural	A1	360.0	60.0	4.8	300.0	3.12	21	Standard Cyclic
	A2*			3.5	300.0	1.97	150	Constant, $2\delta_y$
	A3*			4.8	300.0	4.00	26	Constant, $3\delta_y$
	A4*			4.8	300.0	5.33	9	Constant, $4\delta_y$
	A5*			4.8	300.0	6.67	4	Constant, $5\delta_y$
Quarter Scale Flexural	C1	54.0	12.0	0.5	11.5	2.88	30	Standard Cyclic
	C2			0.5	11.5	2.77	150	Constant, $2\delta_y$
	C3			0.75	11.5	4.17	26	Constant $3\delta_y$
	C4			0.75	11.5	5.56	9	Constant, $4\delta_y$
	C5			0.75	11.5	6.94	4	Constant, $5\delta_y$
	C6			0.75	14.0	2.69	N/A	Random Cyclic
	C7			0.75	14.0	2.79	N/A	Random Cyclic
	C8			0.75	14.0	3.09	N/A	Random Cyclic

* Denotes analytically simulated test (units = inch, kips)

The fatigue-based models demonstrate, as a group, why they show such promise. Each increments damage gradually through the initial reversals with damage increasing more rapidly as higher amplitude cycles are experienced. This behavior is consistent with observed column performance. Interestingly, Fatigue-1 and Fatigue-3 adequately predict damage to the full-scale flexural and shear columns but diverge somewhat on the quarter-scale test. Fatigue-3 overestimates damage for this test while Fatigue-1 under-predicts it.

2.4.2 Constant Amplitude Loading

Tables 2-4 to 2-7 and Figures 2-4 to 2-7 provide information on damage model performance for tests performed under constant amplitude cycling of from $2\delta_y$ through $5\delta_y$. Recall that for each of the constant amplitude tests, only analysis of the quarter-scale column is substantiated with actual test data (Cases C2 - C5). Constant amplitude testing of the full-scale flexural columns (Cases A2 -A5) was analytically simulated.

2.5 Summary

This section summarized the application of several damage models to experimental data. Test data consisted of cyclic tests of circular bridge columns. Constant amplitude and variable amplitude tests were considered in the evaluation. Sensitivity of the selected damage models to model variables were first investigated. Following calibration of the experimental results using IDARC, a series of damage evaluations using the different models were carried out. It was generally concluded that fatigue-based models can be used with greater reliability than all the other types of models considered in this phase of the study. Since fatigue failure in bridge columns is controlled primarily by the fatigue behavior of the longitudinal reinforcement and the effects of confining steel, it was considered essential to gain additional insight into different aspects of constituent material behavior before embarking on the development of a new damage model for reinforced concrete. The first step in this undertaking is detailed in the remainder of this report.

Table 2-3 Peak Cumulative Damage for Circular Columns Subjected to Standard Cyclic Loading, Selected Damage Models

	Hybrid	Softening	Energy	Fatigue-1	Fatigue-2	Fatigue-3
Full Scale Flexural	0.96	0.84	0.99	0.88	0.86	1.13
Full Scale Shear	1.13	0.93	0.93	1.28	0.41	0.86
Quarter Scale Flexural	1.15	0.87	0.99	0.68	0.95	1.65

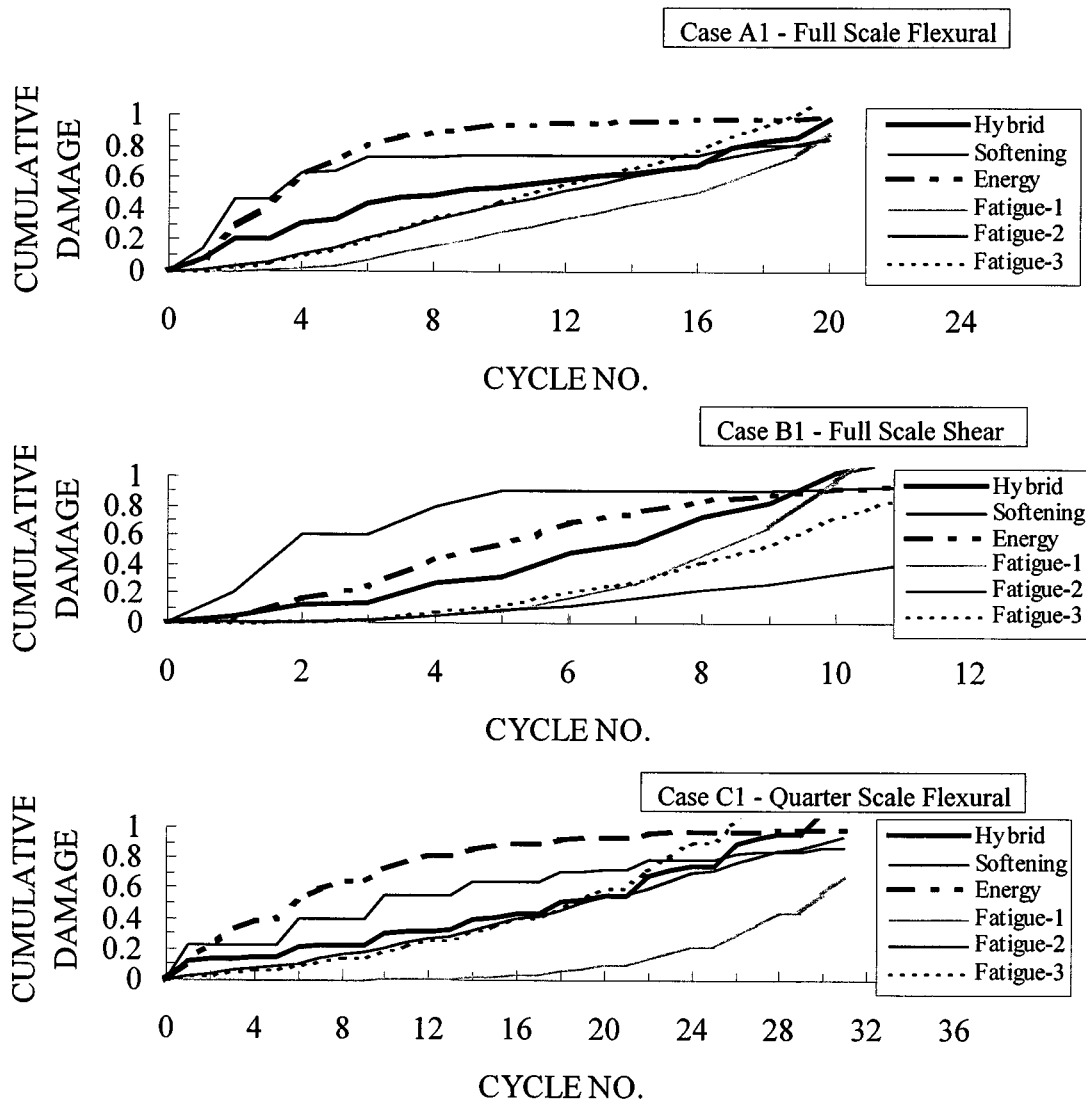


Figure 2-3 Cumulative Damage to Circular Columns, Standard Cyclic Loading, Selected Damage Models

Table 2-4 Peak Cumulative Damage for Circular Columns Subjected to Constant Amplitude Cyclic Loading, $2\delta_y$, Selected Damage Models

	Hybrid	Softening	Energy	Fatigue-1	Fatigue-2	Fatigue-3
Full Scale Flexural	1.50	0.71	1.00	0.61	1.00	1.46
Full Scale Shear	1.37	0.87	0.98	1.19	1.00	0.72
Quarter Scale Flexural	1.67	0.81	1.00	0.69	1.00	1.92

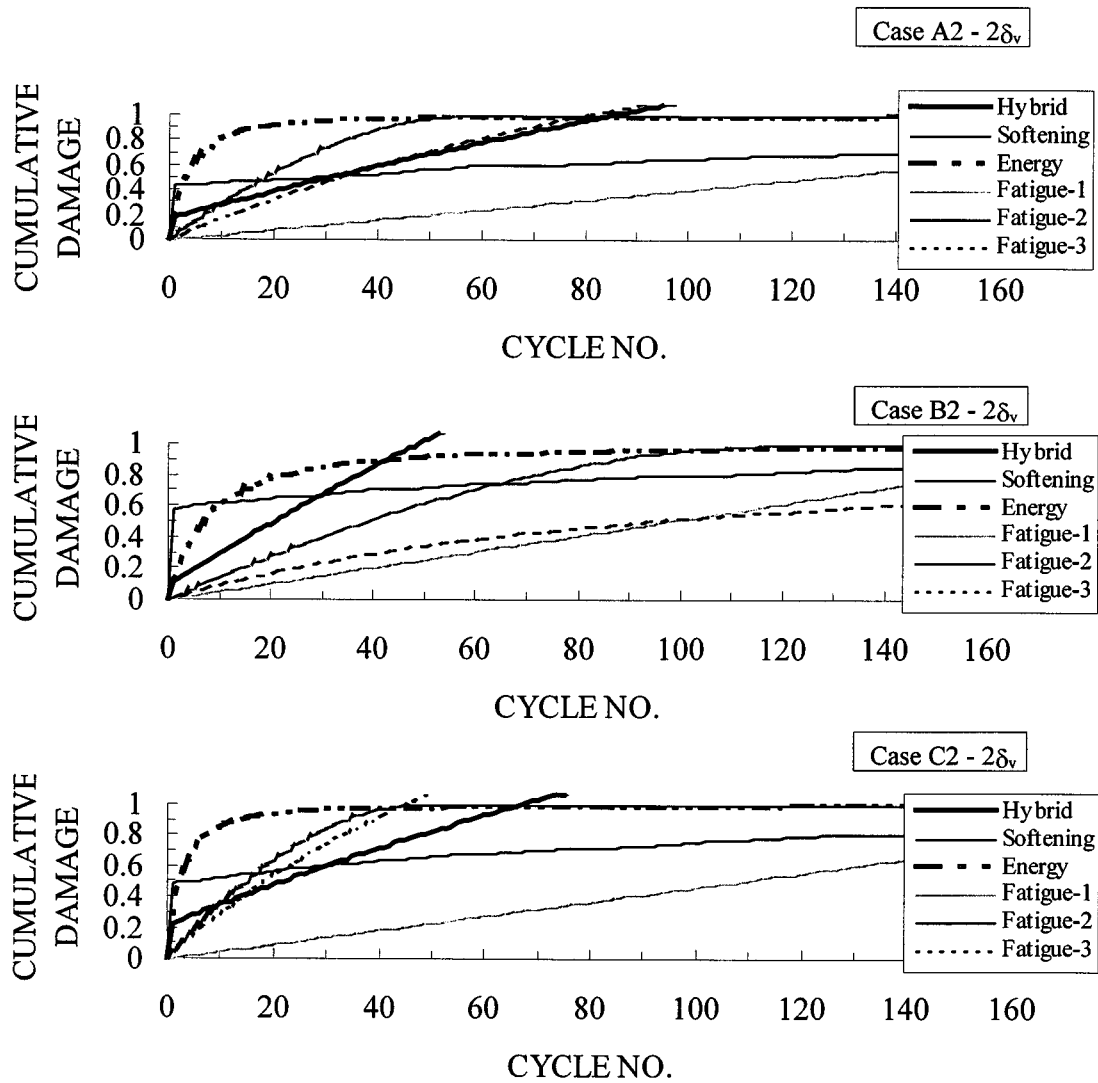


Figure 2-4 Cumulative Damage to Circular Columns, Constant Amplitude Loading, $2\delta_y$, Selected Damage Models

Table 2-5 Cumulative Damage for Circular Columns Subjected to Constant Amplitude Cyclic Loading, $3\delta_y$, Selected Damage Models

	Hybrid	Softening	Energy	Fatigue-1	Fatigue-2	Fatigue-3
Full Scale Flexural	0.95	0.79	0.99	1.12	0.98	1.37
Full Scale Shear	0.89	0.8	0.9	0.41	0.49	0.44
Quarter Scale Flexural	1.25	0.86	0.99	1.44	1	2.75

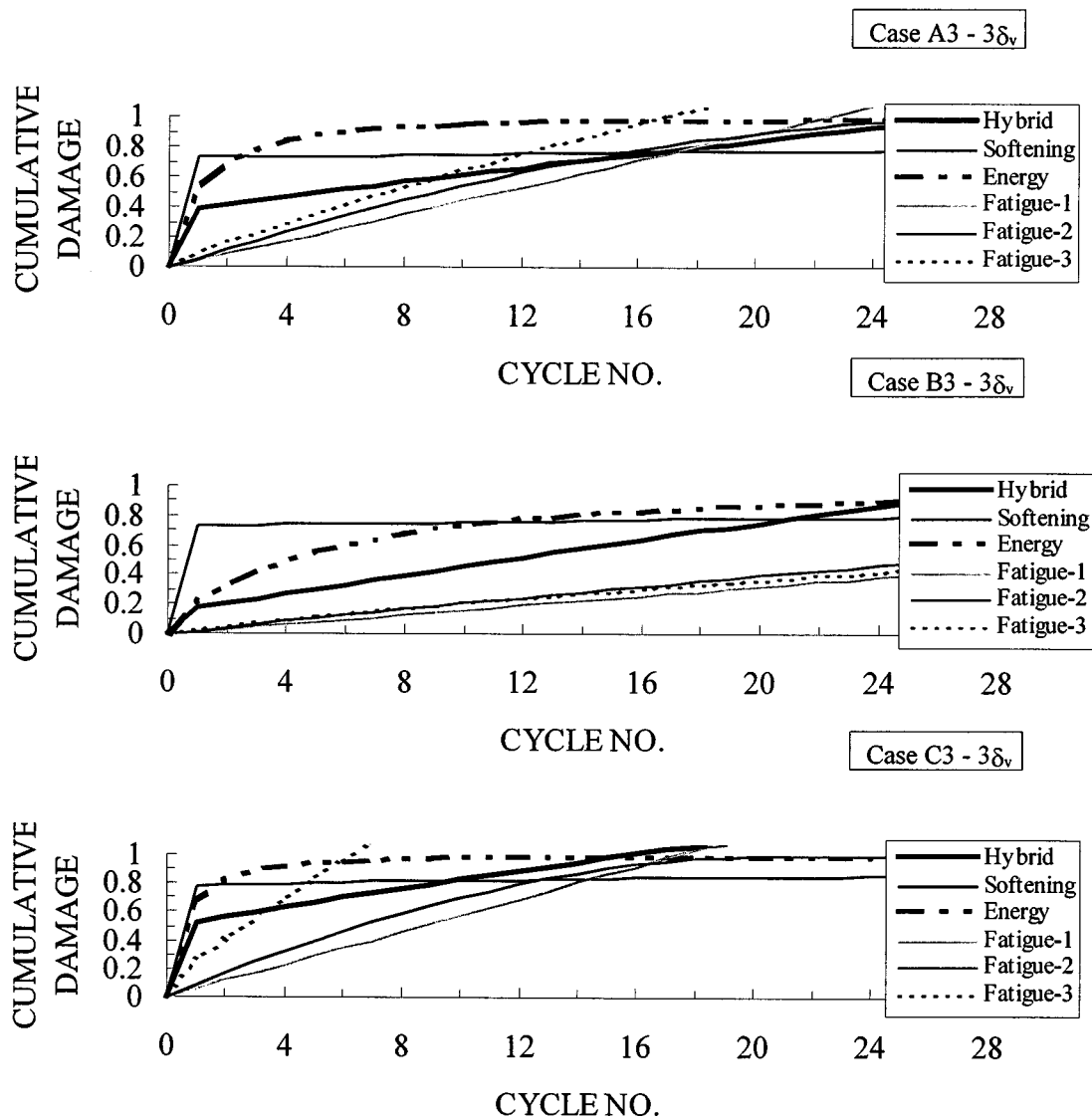


Figure 2-5 Cumulative Damage to Circular Columns, Constant Amplitude Loading, $3\delta_y$, Selected Damage Models

Table 2-6 Peak Cumulative Damage for Circular Columns Subjected to Constant Amplitude Cyclic Loading, $4\delta_y$, Selected Damage Models

	Hybrid	Softening	Energy	Fatigue-1	Fatigue-2	Fatigue-3
Full Scale Flexural	0.75	0.81	0.97	0.81	0.58	0.9
Full Scale Shear	0.53	0.81	0.77	0.29	0.22	0.29
Quarter Scale Flexural	1.25	0.86	0.99	0.95	0.74	1.99

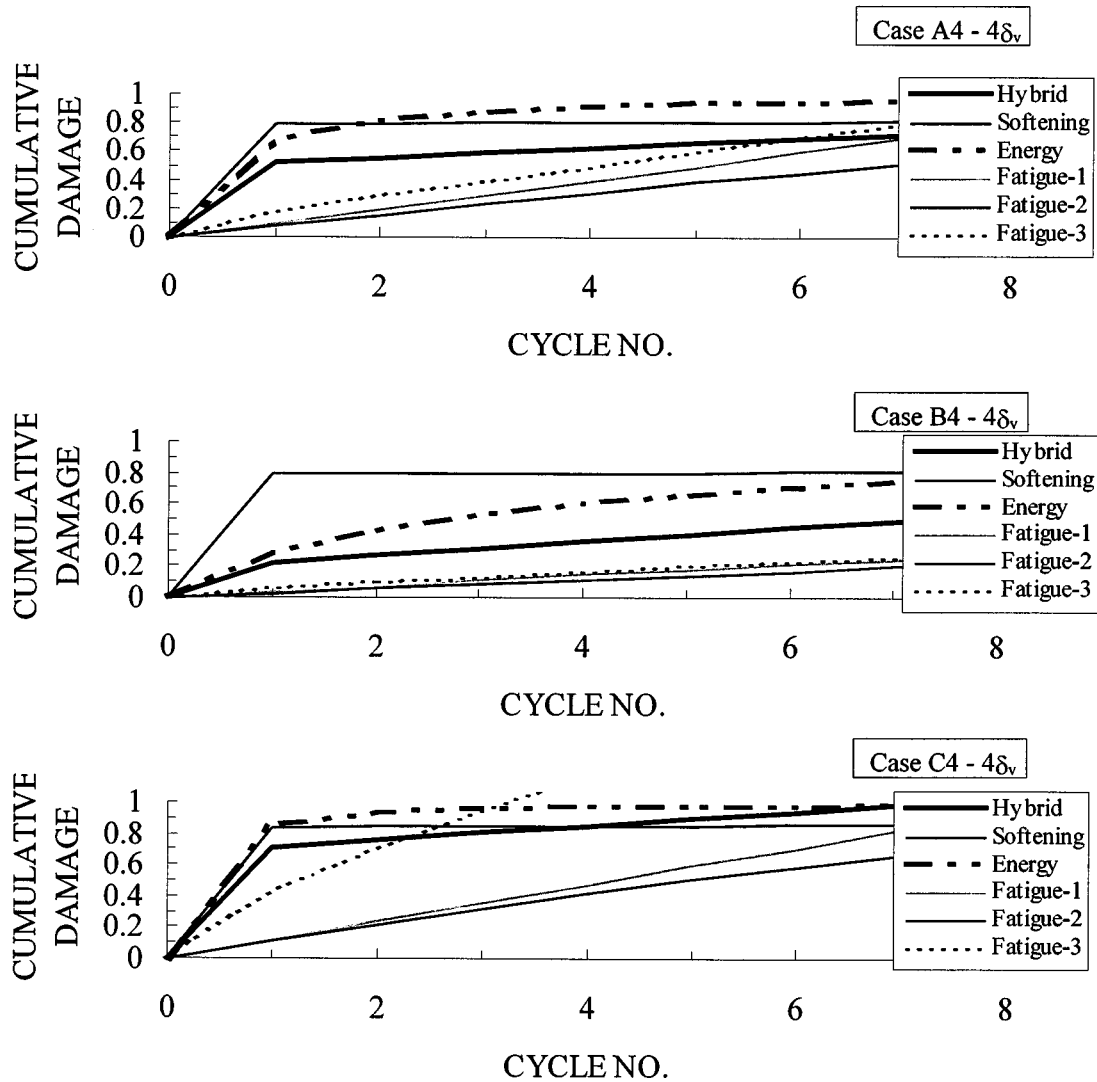


Figure 2-6 Cumulative Damage to Circular Columns, Constant Amplitude Loading, $4\delta_y$, Selected Damage Models

Table 2-7 Peak Cumulative Damage for Circular Columns Subjected to Constant Amplitude Cyclic Loading, $5\delta_y$, Selected Damage Models

	Hybrid	Softening	Energy	Fatigue-1	Fatigue-2	Fatigue-3
Full Scale Flexural	0.79	0.85	0.96	0.72	0.4	0.75
Full Scale Shear	0.46	0.85	0.69	0.24	0.16	0.24
Quarter Scale Flexural	1.06	0.88	0.99	0.79	0.53	1.86

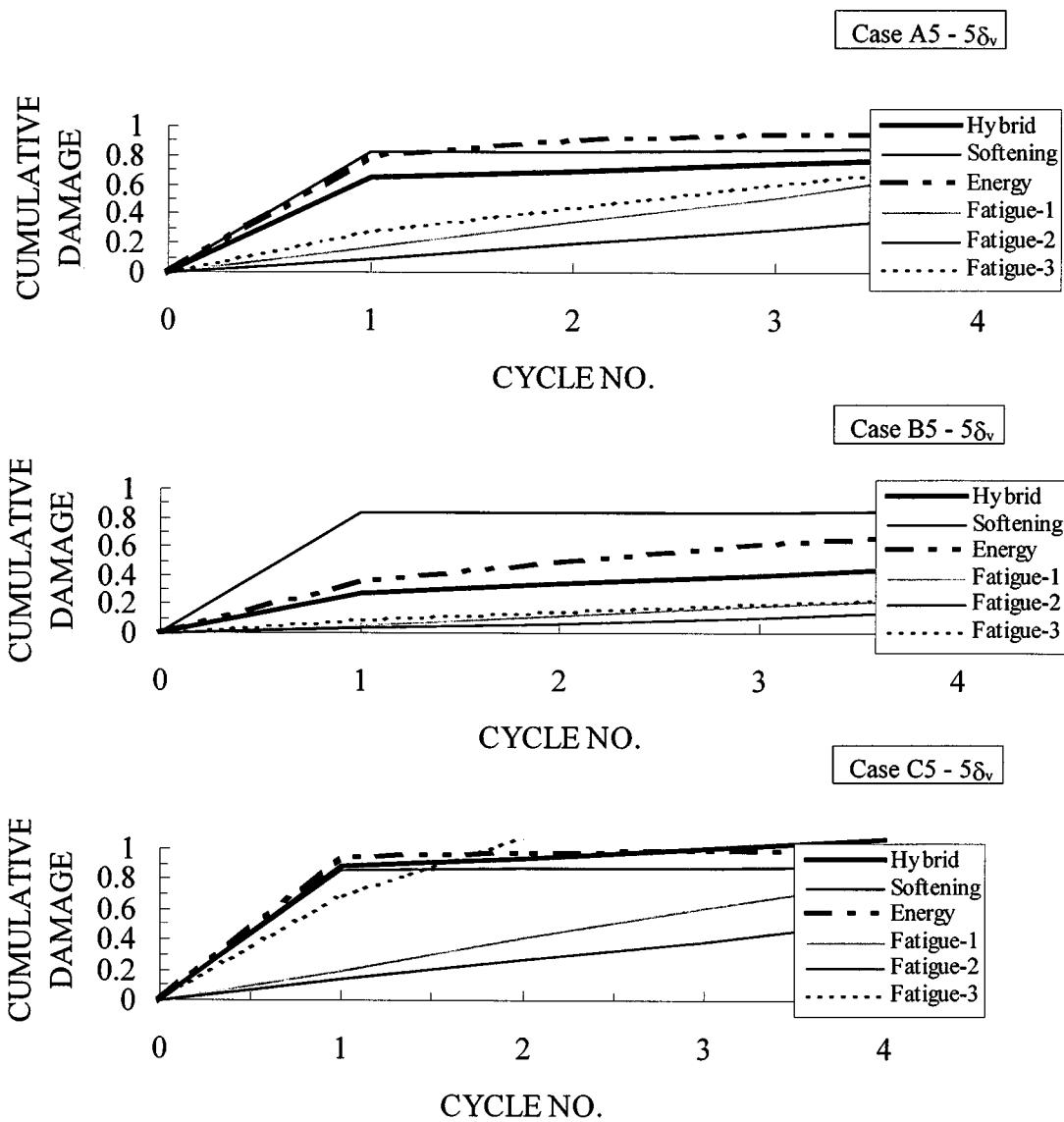


Figure 2-7 Cumulative Damage to Circular Columns, Constant Amplitude Loading, $5\delta_y$, Selected Damage Models

SECTION 3

DESIGN OF EXPERIMENTAL SETUP FOR LOW-CYCLE FATIGUE TESTING OF REINFORCING BARS

Initial findings from the analytical study presented in the previous section indicate that most of the existing fatigue-based models are not based on test data generated from low-cycle fatigue tests of reinforced concrete or their constituent materials. Hence, they do not consistently predict the cumulative damage process though, conceptually, they possess the right attributes of a reliable model. Calibrating the material constants in a fatigue-life expression requires experimental data. It was, therefore, concluded that a more detailed understanding of the low-cycle fatigue behavior of reinforcing bars was essential to the development of a predictive damage model for bridge columns. Much of the effort for the remainder of the project was devoted to the planning and design of a test set-up to facilitate the testing of standard reinforcing bars under reversed cyclic loading. Details of this effort are summarized here.

3.1 Background

Low cycle fatigue (LCF) behavior is characterized by high amplitude strain reversals that result in material failure after relatively few cycles (<1000). During a seismic event, reinforced concrete (RC) structures are subjected to strong ground motions that induce similar cyclic inelastic deformations in steel reinforcement. While proper reinforcement detailing in critical regions of a structure (plastic hinge regions) may prevent collapse during large displacement responses, structures are still susceptible to cumulative low cycle fatigue damage. The goal of this part of the research is to isolate the damage sustained by steel reinforcement in a RC structure due to seismic loading and apply this information in the assessment of overall damage following a seismic event.

3.2 Review of Literature

It is estimated that 80 percent of all machine metal failures are due to fatigue (Smith, 1990). As a result, numerous books and journals are dedicated to the topic. The intent of this section is to describe the fundamental concepts of fatigue and damage that pertain to this study of concrete reinforcement.

3.2.1 The Fatigue Process

Fatigue failures occur due to cyclic loading at a stress (or strain) level that is less than what is required to fail the material in a single application of the load. The fatigue-life of a material is defined as the number of cycles at specific deformation amplitudes resulting in failure. Figure 3-1 represents a fatigue-life curve for a typical engineering alloy. As the level of deformation or load decreases, the number of cycles to failure increases. For materials that have elastic-plastic properties, such as reinforcing steel, the fatigue-life curve can be broken up into two distinct regions. The first describes low-cycle fatigue behavior (less than 1000 cycles to failure) and is controlled by plastic deformations. The second describes high-cycle fatigue behavior and is controlled primarily by elastic deformations. Once the stress or deformation level drops below the fatigue limit, an unlimited number of cycles may be applied without experiencing fatigue failure.

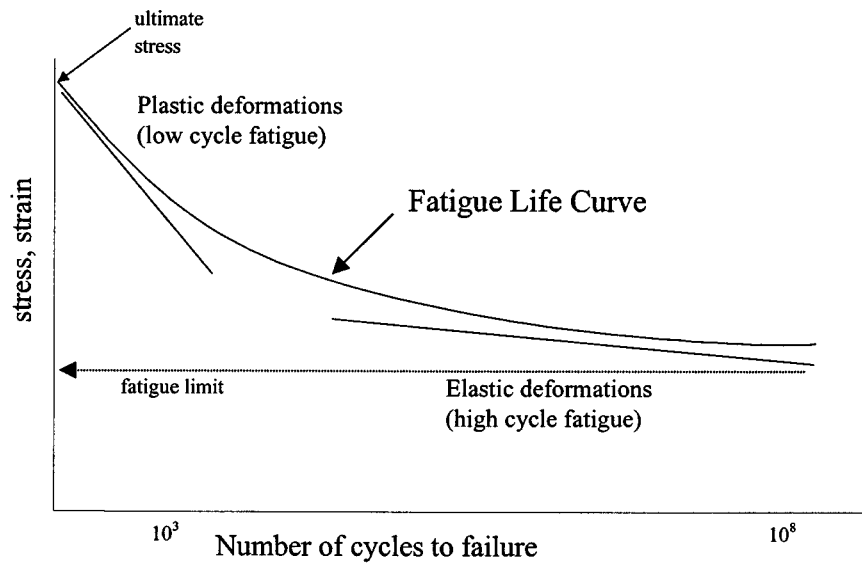


Figure 3-1 Typical Fatigue-life Curve for an Engineering Alloy

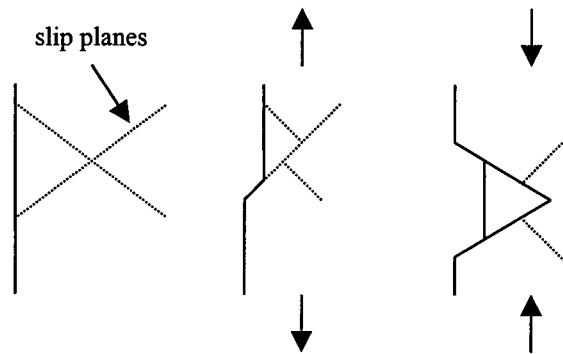


Figure 3-2 Slipband Extrusion and Initial Crack Formation (Smith, 1990)

The first stage in the fatigue process is the formation of a fatigue crack, usually at or near the surface of a specimen. Irreversible plastic strains may occur as a result of the imposed deformations or stress concentrations (due to surface imperfections or geometric features). These

deformations lead to the creation of *slipband extrusions* (shown in Figure 3-2) and *slipband intrusions* that eventually manifest into cracks under repeated cyclic loading. Once the crack has formed, it will continue to propagate until there is insufficient surface area to resist the load, and ductile fracture will occur.

3.2.2 High Cycle Fatigue in Concrete Reinforcement

Under normal service load conditions, the response of all members in a structure is expected to remain elastic. The cyclic nature of loading in bridge structures due to vehicle action, however, still allows for the failure of flexural elements from fatigue. To ensure that fatigue failures do not occur in RC bridges, the following formula is used to determine the allowable stress range permissible in main longitudinal reinforcement (Corley et al, 1978):

$$f_f = 21 - 0.33 f_m + 8 \frac{r}{h} \quad (3-1)$$

where: f_f = allowable stress range due to live load plus impact (ksi)
 f_m = minimum stress level, tension positive (ksi)
 r/h = ratio of base radius to height of rolled on deformation

Corley's study (1978) was based on 353 RC beams tested under fatigue loading. Size of beam, size of bar, grade of bar, deformation geometry, mean stress, and stress ranges were all varied. The conclusion most relevant to the present study is that geometric properties of the reinforcing bar have a significant effect on the fatigue-life. Even the manufacturer's identification markings were noted as a potential cause of reduced fatigue resistance.

3.2.3 Low-cycle Fatigue in Concrete Reinforcement

A series of low-cycle fatigue tests were performed at the State University of New York, Buffalo, in 1994 (Mander et al, 1994). Both Grade 40 and high strength prestressing bars were examined. Due to the presence of rolled-on deformations and the inelastic buckling that occurs during

compression cycles, it was decided to leave the original cross-section of the specimen in tact. This requirement posed a considerable challenge in the design of the test setup. The transfer of forces to the specimen in such a way that the fatigue failure occurred away from the gripping mechanism required an elaborate procedure. The unsupported length (s) of the specimens tested was equivalent to six bar diameters (d_b). s/d_b ratios of 6,8, and 9 were examined with uni-axial compression tests in order to determine how this ratio affects the loss of strength at high compressive strains. Results indicated that s/d_b ratios larger than six led to a reduction in strength below the yield value as large compressive strains (approximately 0.06) were imposed. This was a result of severe inelastic buckling. Previous research (Mander et al, 1988) indicates that well confined concrete is capable of achieving strains on the order of .06 without failure. From this, Mander concludes that center to center transverse reinforcement spacing greater than six d_b may be inadequate. This conclusion also served as the basis for using an unsupported length of six d_b (9.5 cm for #16m Grade 40 rebar) in the tests.

Deformation measurements were made using a custom-built aluminum extensometer. This device was designed to monitor deformations over the central 1.875 inches of the specimen ($s/2$). Assuming completely fixed end conditions, this gage length corresponds to the area between inflection points of a double-curvature buckling profile. Results have been presented for 10 low-cycle fatigue experiments on Grade 40 reinforcement and 22 experiments on high strength prestressing bar. It was shown that the two material types had different low-cycle fatigue properties and that the high strength prestressing bar generally offered greater resistance to fatigue.

Mander used two separate criteria to identify failure (occurring after $2N_f$ cycles). The first, used for small amplitude strain ranges ($< .02$), involved monitoring the ratio of stress developed at the first tension peak (f_0) to the stress developed at subsequent tension peaks (f_i). After the first few cycles of strain hardening, the ratio f_i/f_0 remained stable. Upon the formation of a fatigue crack, a marked drop in this ratio occurred and the specimen was considered to have failed. The second method, used for strain amplitudes $> .02$, relied on the visual observation of fatigue cracks and a rapid loss of strength prior to achieving the peak tensile strain (negative slope on the stress vs.

strain curve). Mander also reported that the initiation of a fatigue crack was quickly followed by complete failure of the specimen.

Several existing fatigue-life models were applied to these results. The objective of these models is to provide a mathematical relationship between the imposed deformations (strain amplitudes or cumulative energy) and the number of cycles to failure. Based on experimental data, material constants (such as ϵ'_f and c in equation 1) may be established. The following fatigue-life models were utilized by Mander:

1. Coffin - Manson equation for plastic strain amplitude (Coffin, 1954; Manson 1953):

$$\epsilon_{ap} = \frac{\Delta\epsilon_p}{2} = \epsilon'_f (2N_f)^c \quad (3-2)$$

where: ϵ_{ap} = plastic strain amplitude
 $\Delta\epsilon_p$ = total plastic strain range
 $2N_f$ = number of cycles to failure
 ϵ'_f and c = material constants

2. Koh and Stephens' equation for total strain amplitude (Koh and Stephens, 1991):

$$\epsilon_a = \frac{\Delta\epsilon}{2} = M (2N_f)^m \quad (3-3)$$

where: ϵ_a = total strain amplitude
 $\Delta\epsilon$ = total strain range ($\epsilon_{\max} - \epsilon_{\min}$)
 M and m = material constants

3. Modified SWT equations for total strain amplitude (Koh and Stephens, 1991) and for plastic strain amplitude (Lorenzo and Laird, 1984):

$$\epsilon_a f_{mx} = C(2N_f)^{\gamma} \quad (3-4)$$

$$\epsilon_{ap} f_{mx} = L(2N_f)^l \quad (3-5)$$

where: f_{mx} = maximum tensile stress at the half-life of each specimen

C and γ = material constants for total strain model

L and l = material constants for plastic strain model

4. Energy based models proposed by Mander et al (1994):

$$W_{fT} = W_a (\varepsilon_a)^p \quad (3-6)$$

$$W_{fT} = W_{ap} (\varepsilon_{ap})^q \quad (3-7)$$

$$W_{fT} = W_{fa} (f_{mx} \varepsilon_a)^r \quad (3-8)$$

$$W_{fT} = W_{fap} (f_{mx} \varepsilon_{pa})^s \quad (3-9)$$

where: f_{mx} = maximum tensile stress achieved in each specimen

W_{fT} = total strain energy to failure

$W_a, W_{ap}, W_{fa}, W_{fap}, p, q, r,$ and s = material constants

Table 3-1 Fatigue-life Model Curve Fits (Mander et al, 1994)

Model	Equation Number	Curve Fit	r^2
Coffin - Manson	1	$\varepsilon_{ap} = .0777(2Nf)^{-.486}$.984
Koh - Stephens	2	$\varepsilon_a = .0791(2Nf)^{-.448}$.985
Modified SWT (total strain)	3	$f_{max} \varepsilon_a = 51.6(2Nf)^{-.541}$.991
Modified SWT (plastic strain)	4	$f_{max} \varepsilon_{ap} = 50.6(2Nf)^{-.581}$.988
Energy - (total strain)	5	$W_{fT} = 6.72(\varepsilon_a)^{-.961}$.914
Energy - (plastic strain)	6	$W_{fT} = 8.00(\varepsilon_{ap})^{-.884}$.911
Energy - (stress X total strain)	7	$W_{fT} = 1,840(f_{max} \varepsilon_a)^{-.961}$.922
Energy - (stress X plastic strain)	8	$W_{fT} = 1,456(f_{max} \varepsilon_{ap})^{-.745}$.918

This series of tests served as an important reference for the experiments conducted in the present study. However, Mander's tests were limited to small bar sizes (#16 metric designation) not typically used for longitudinal reinforcement and only involved constant amplitude strain histories. As a result, it is believed that further experimental research on the low-cycle fatigue behavior of concrete reinforcement is necessary to gain a better insight into the damage process and failure of reinforced concrete structures under seismic loads.

3.3 Test Setup

In order to simulate the effects of seismic loading on the concrete reinforcement (rebar), the following test setup characteristics were identified:

- Tensile and compressive loading
- Accommodate full size specimens typically used for longitudinal reinforcement
- No physical alteration of the specimen over a given test length (six d_b)
- Apply constant and variable amplitude strain histories to the specimen

The following considerations were also critical in the development of the test program:

- Use of existing facilities at NIST
- Re-usable gripping mechanism for transferring force to rebar

To induce low cycle fatigue behavior, the axial loads transferred to the specimen had to be sufficiently large to yield the specimen. Mill report data (Table 3-2) provided for each bar size (ASTM Designation A 615/A 615M – 96a, Grade 60[420] reinforcement) indicated an ultimate stress of the material ranging from 655 to 725 MPa. This translated into a minimum design force of 467 kN (105,000 lbf) for each component of the test setup. A factor of safety of two was employed to ensure that any dynamic response of the system (resulting from the rapid release of energy at specimen failure) would be safely accommodated.

Table 3-2 Mill Report Data for Rebar Specimens

Bar Size metric (std.)	Diameter mm (in.)	Area mm ² (in. ²)	Yield Stress MPa (ksi)	Ultimate Stress MPa (ksi)	% Elongation in 203 mm
19 (#6)	19.1 (.750)	284 (.44)	420 (60)	620 (90)	9
22 (#7)	22.2 (.875)	387 (.60)	420 (60)	620 (90)	8
25 (#8)	25.4 (1.00)	510 (.79)	420 (60)	620 (90)	8

3.3.1 Hydraulic Actuator and Reaction Frame

Typically, fatigue experiments are performed on specimens that are notched or machined down to ensure that all damage and crack propagation occurs in a specific region. Minimum cross-section diameters of such specimens (shown in Figure 3-3) are on the order of 5 - 10 mm and are chosen based on the strength of the material. As a result, fatigue-testing machines (capable of both tensile and compressive loading) usually have very limited force capacity. To accommodate the force requirements of specimens with diameters up to 25 mm (and for future experimental work on specimens with diameters up to 43 mm), a 2700 kN (tension/compression) servo-driven hydraulic actuator and reaction frame system was identified as the only viable alternative. In this system, two vertical columns (W12x87) are tied down to the facility's strong floor, and a main crossbeam (composed of 2 - W36x170 sections) provides a reaction point for the top of the specimen. The hydraulic actuator rests on two box beams, also tied down to the strong floor, and imposes deformations by displacing the bottom of the specimen (shown in Figure 3-4). The load frame is completed by a short W12x190 section aligned perpendicular to the main crossbeam. This member acts to transfer load directly from the specimen gripping mechanism to the main crossbeam.

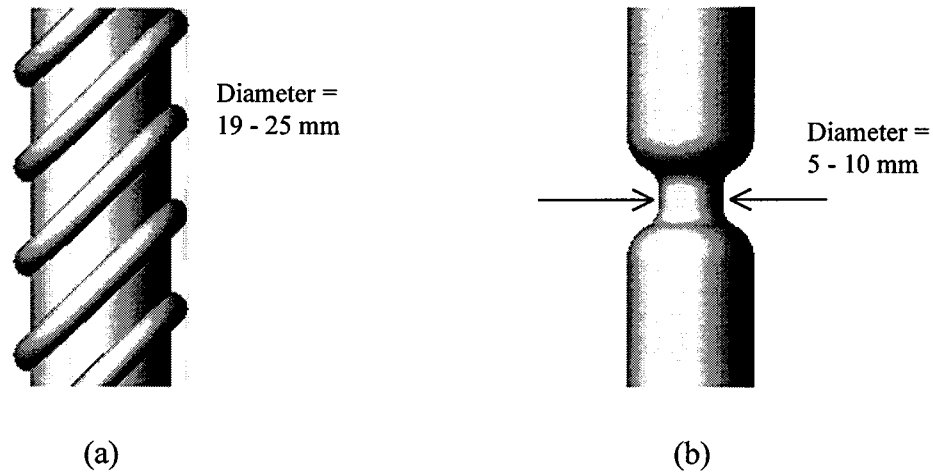


Figure 3-3 (a) Gage length of rebar specimen used in present testing (b) Typical fatigue test specimen used in conventional testing

Figures 3-4 and 3-5 provide a general schematic drawing of the load frame and hydraulic actuator system. The vertical columns are oriented such that strong axis bending occurs with deflections in the east-west direction. Since the loading was expected to be entirely concentric, little attention was given to providing lateral support in the north-south direction (perpendicular to page). Unfortunately, weak axis bending in the vertical columns led to severe north-south deflections of the main crossbeam when the specimen was subjected to compressive forces.

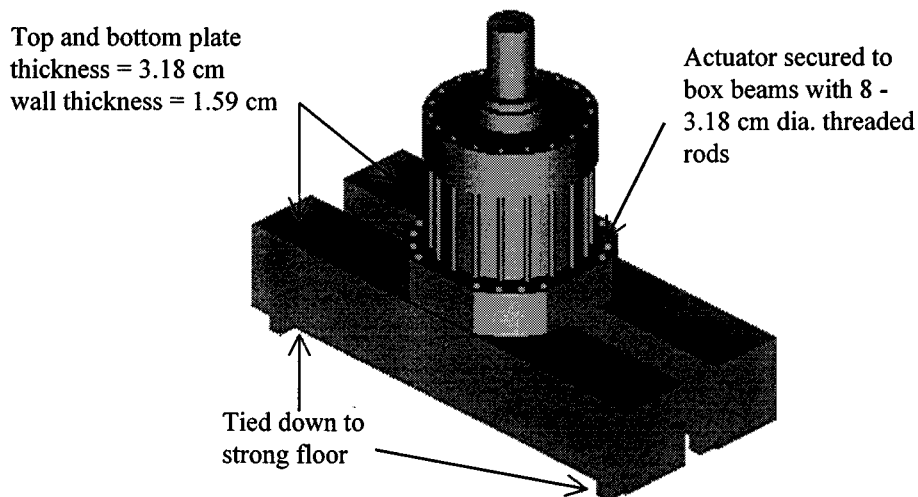


Figure 3-4 Actuator and box beams anchored to strong floor

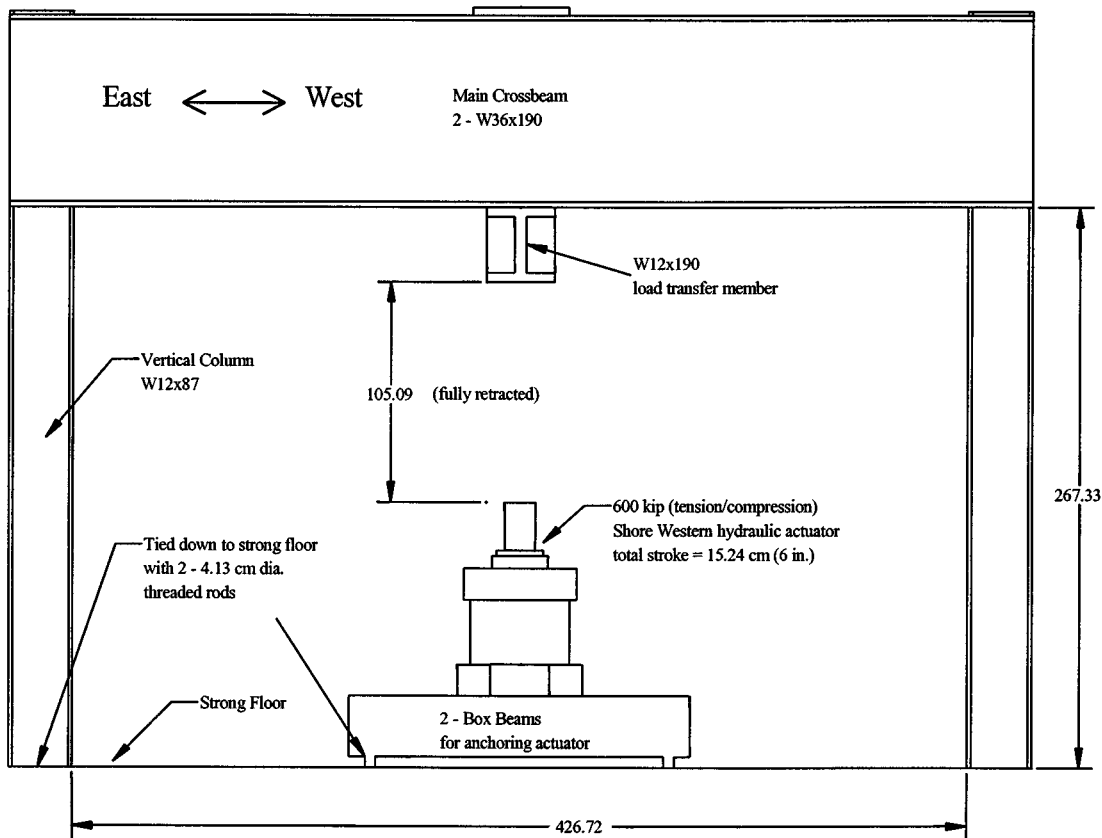


Figure 3-5 General schematic of load frame and hydraulic actuator (dimensions in cm)

3.3.2 Force Transfer to Specimen

In order to generate an inelastic response in each test specimen, sufficient axial force must be transferred via shear stress over a specific development length (illustrated in Figure 3-6). It is of utmost importance that any damage and subsequent fatigue failure occur in the specimen gage length away from the gripping mechanism. Should the gripping mechanism lose its ability to transfer force, yielding of the specimen was unlikely and the test could not be completed. The task is usually accomplished by either increasing the cross-sectional area of the specimen throughout the development length or decreasing the cross-sectional area within the specimen's gage length.

A pilot study was conducted in order to develop a suitable means for transferring force to the specimen gage length. The concept under consideration is best described as swaging. A soft, easily deformed material is placed between the specimen and large gripping blocks to act as a force transfer medium. The assembly is placed in a compressive testing machine and a force is applied such that the deformations present on the rebar impart their pattern on one side of the medium and machined deformations on the gripping block impart their pattern on the opposite side. The assembly is then bolted together and the gripping blocks are connected to the hydraulic actuator and reaction frame.

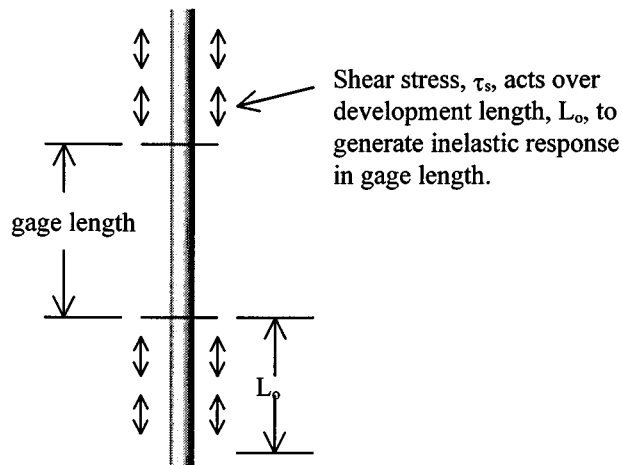


Figure 3-6 Force transfer to specimen gage length

A simple force equilibrium equation was used to determine the required development length:

$$P_u = \int \tau_s dA \quad (3-10)$$

where: P_u = total factored force required to fail specimen

A = contributing area of transfer media

τ_s = shear stress developed in transfer media

Assuming a shear stress distribution as shown in Figure 3-7 and that only 40 percent of the specimen's surface area participates in the force transfer process, equation 2-1 may be expressed as:

$$P_u = \frac{1}{2} \tau_{mx} L_o (0.4) P_s \quad (3-11)$$

where: P_s = perimeter of specimen

L_o = required development length

τ_{mx} = maximum shear stress developed in transfer media

2024 - T4 aluminum (Al) was chosen as the force transfer medium. The ultimate shear stress of this material is approximately 282 MPa. To avoid the potential for pullout, the allowable maximum shear stress was set at 70 percent of this value, or 198 MPa. P_u was obtained by increasing the force required to fail each specimen by a factor of 1.4.

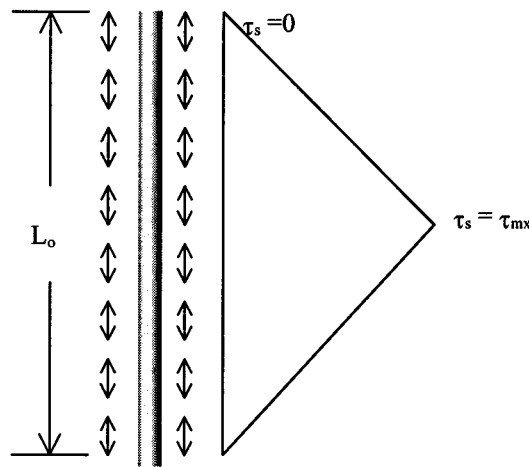


Figure 3-7 Assumed shear stress distribution within development length

The concept was tested on a #16 (metric designation) Grade 60 rebar (Figure 3-8). The force required to fail this specimen was approximated at 143.3 kN, resulting in a development length of 10.16 cm. Two pieces of Al 0.318 cm thick and 1.91 cm wide were used as the force transfer medium. Figure 3-8 provides a detailed drawing of the gripping block (machined from AISI 1018 steel) used in the experiment. A uni-axial tension force was applied to the specimen using

a 266 kN capacity SATEC Universal Testing Machine (UTM). The fabricated blocks gripped only one end of the specimen with the other end held by standard tension grips.

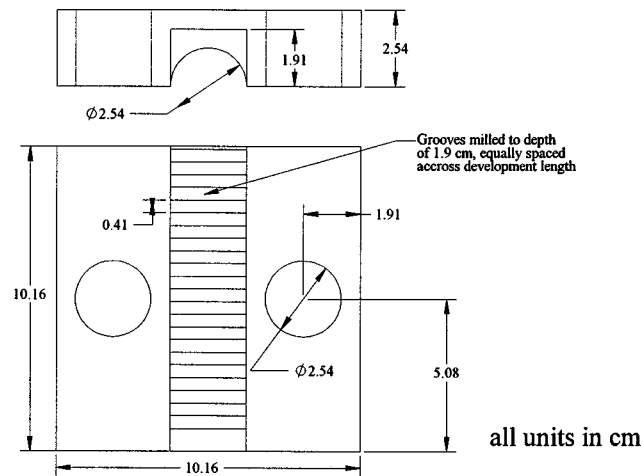


Figure 3-8 Detail drawing of pilot grip for use with Grade 60, #16 rebar

Results from this experiment indicated that the swaging concept is an effective means of transferring axial force to deformed rebar. The ultimate strength of the specimen was realized without any pullout or slip in the gripping mechanism. Another very important observation was that the milled-out deformations in the gripping block were damaged during the swaging process. While this did not affect its ability to transfer force in this experiment, it was felt that repeated swaging might lead to a reduction in the grip's performance. The following section describes modifications made in the design of the prototype grip for implementation into the test setup.

3.3.3 Prototype Rebar Grip

The prototype rebar grip was designed to accommodate bar sizes ranging from 19 to 29 mm in diameter. A required development length of 20.3 cm was determined using the procedure outlined in the pilot study. To avoid damaging the grips during the swaging process, the deformations were fabricated with a high-hardness weld diode. This ensures that the aluminium force transfer medium is the only component to undergo inelastic deformations during swaging.

Flanges were also added that enable the grip assembly to be secured to the reaction frame and hydraulic actuator. The final grip used in the testing is shown in Figures 3-9 and 3-10.

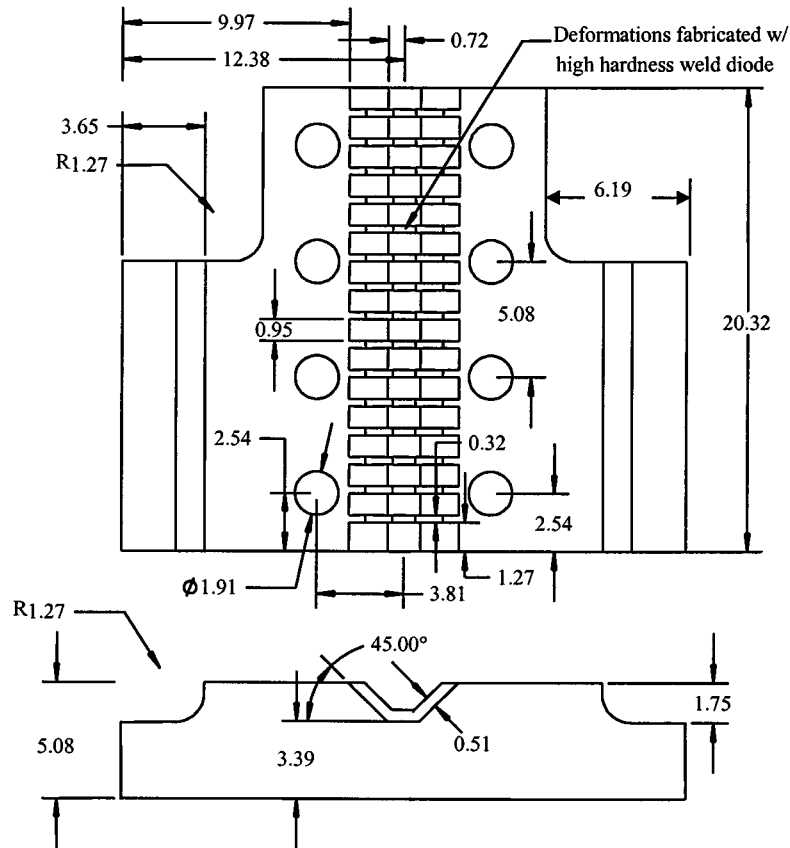


Figure 3-9 Detail drawing of prototype grip (all units in cm)

3.3.4 Load and Deformation Measurements

A 667 kN capacity (tension/compression) load cell was incorporated into the test setup as shown in Figure 3-11. Two adapters, also shown, were required to connect the load cell to the hydraulic actuator and specimen grip assembly. This configuration resulted in problems during testing due to the relative slenderness of the load cell. When high compressive forces develop in the specimen and buckling occurs, the load cell offers limited resistance to lateral deflections.

Unfortunately, this was the only device available with the required tension/compression load capacity.

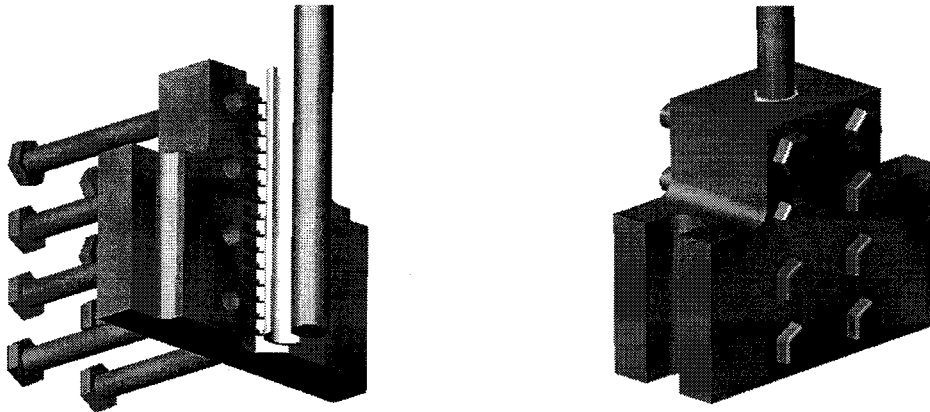


Figure 3-10 Prototype rebar grip

Deformation measurements were made using two types of sensors. Linear variable differential transformers (LVDTs) were mounted to the bottom of the grip assembly and positioned to monitor the relative vertical displacement between grips. Additionally, a standard extensometer with a gage length of 5.08 cm was attached directly to the specimen. The configuration of these devices is illustrated in Figure 3-12.

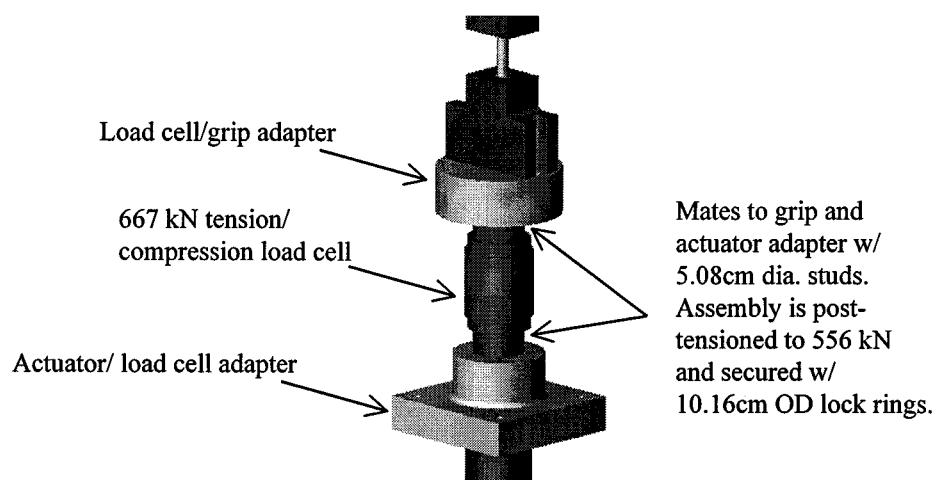


Figure 3-11 Load cell with actuator and grip adapters

3.3.5 Data Acquisition and Control

The most important feature of this test setup is the closed loop active hydraulic control. A target level of deformation (strain) is supplied to the control program, which then decides the required direction of actuator displacement. The actuator is given small increases in command voltage via a servo control box until the desired level of deformation has been obtained. Upon reaching the target strain, the direction of the actuator's displacement is quickly reversed (so as not to overshoot the target). The control program then receives a new target and the process is repeated. This procedure is illustrated in Figure 3-13.

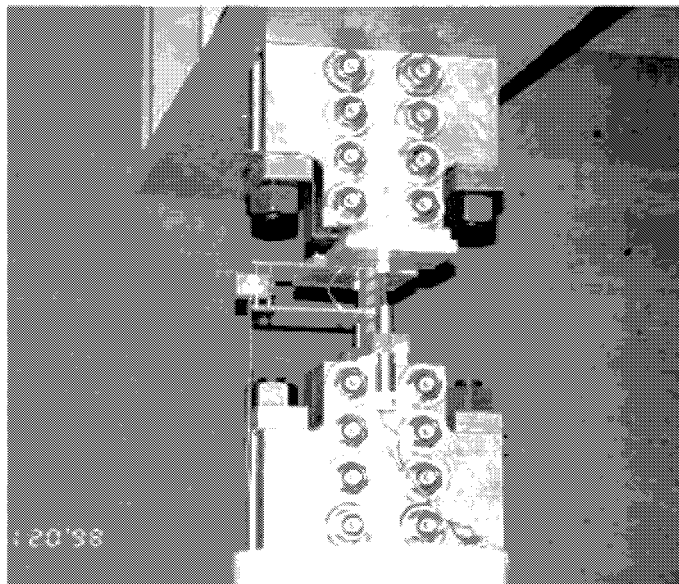


Figure 3-12 LVDTs and extensometer used for deformation measurements

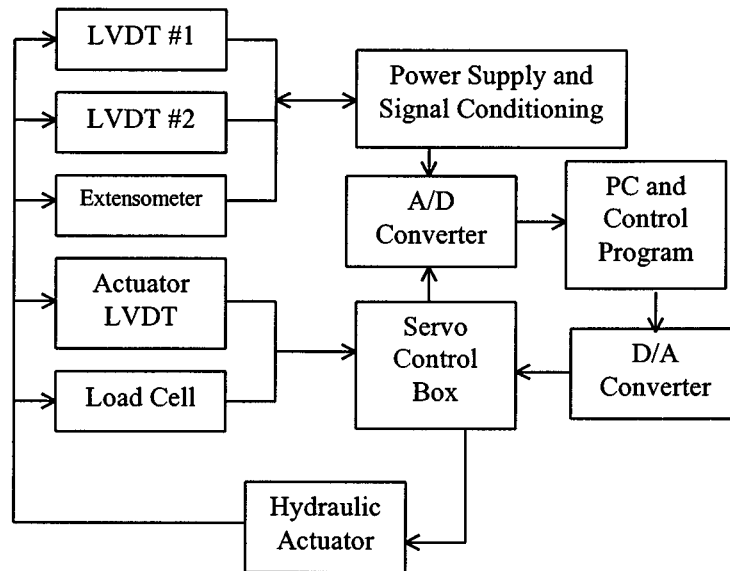


Figure 3-13 Schematic of closed loop hydraulic control

3.4 Summary

A review of the literature on low-cycle fatigue testing of reinforcing bars indicated that the only data set relevant to this study was a series of tests conducted by Mander and co-workers at the University at Buffalo. A brief summary of Mander's tests and findings were presented in this section. Next, details of the experimental setup designed to carry out the proposed fatigue experiments were described. The most important criteria used in the development of the rebar grip was the fact that no physical alteration of the rebar across the gage length was permitted. A preliminary reduced scale model of the grip was first fabricated and proof-tested prior to fabricating the full-scale grip to be used in the fatigue testing. Results of the experimental testing are reported in the following section.

SECTION 4

RESULTS OF FATIGUE TESTS ON REINFORCING BARS

4.1 Constant Amplitude Testing

The purpose of the constant amplitude tests is to establish a fundamental relationship between strain amplitude and the number of cycles to failure. These results will form the basis for the development of a fatigue-life relationship such that behavior under random loading is predictable. A total of 34 constant amplitude tests were performed. Bar sizes tested include #19, #22, and #25 (metric designations). Details of the testing and a summary of the results are presented here.

4.1.1 Specimen Preparation

The first stage of specimen preparation is the deformation of the Aluminium (Al) force transfer medium. A detail drawing of the aluminium used is provided in Figure 4-1. Each end of the grip assembly was placed in a 1330 kN capacity SATEC UTM, and the maximum compressive force is applied transverse to the specimen.

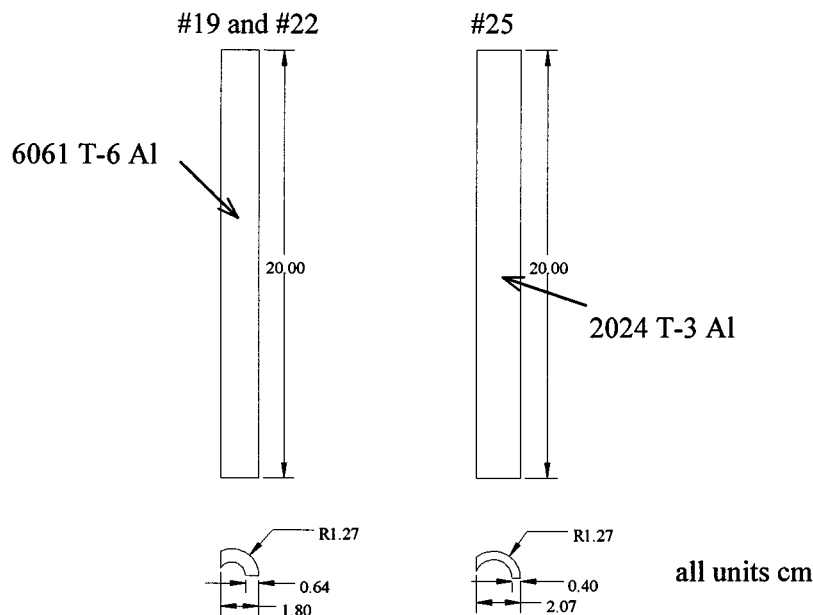


Figure 4-1 Force Transfer Medium Detail

1.91 cm dia. guide pins were placed in the eight bolt holes to ensure that proper grip alignment was maintained during the swaging process. Once the aluminium has been properly deformed, the grip assembly is bolted together with eight 12.7 - 1.91 cm diameter bolts on each end. It is extremely important that the exact alignment achieved during swaging is maintained throughout the assembly process. If done properly, the four pieces of aluminium could be reused on multiple specimens of the same bar size. Figure 4-2 and 4-5 illustrate the main features of specimen preparation.

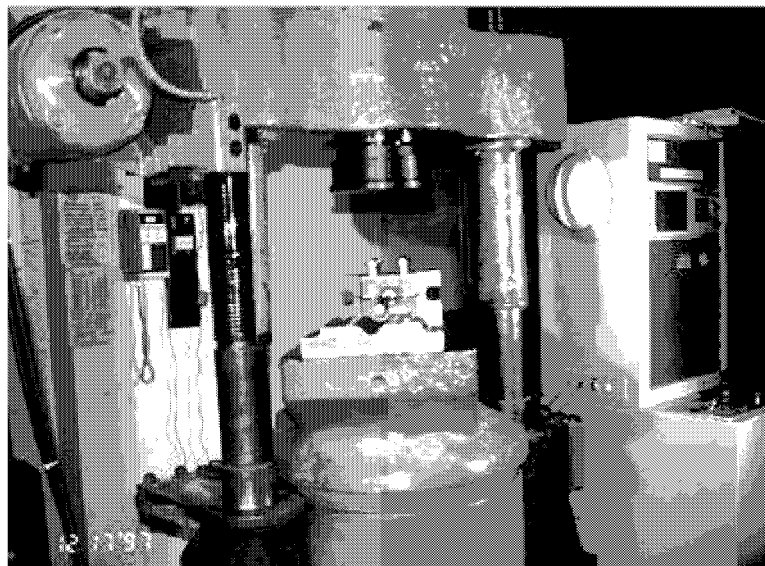


Figure 4-2 Deformation of Force Transfer Media with UTM

4.1.2 Observations and Results

Figure 4-6 provides typical stress vs. strain data recorded during these constant amplitude experiments. In each experiment, the hydraulic control program was provided a target strain value (.025 for experiment #24), and the level of deformation was applied cyclically at the given value. The same rate of deformation was maintained for all experiments at approximately .001 strain/sec. Due to the size of the hydraulic actuator being used, very little could be done to alter this rate of loading. The initial slope of the stress vs. strain graphs was roughly 200,000 MPa for all tests indicating that the experimental setup was working as designed and that the deformations of the aluminum were effectively excluded from the measured rebar strains.

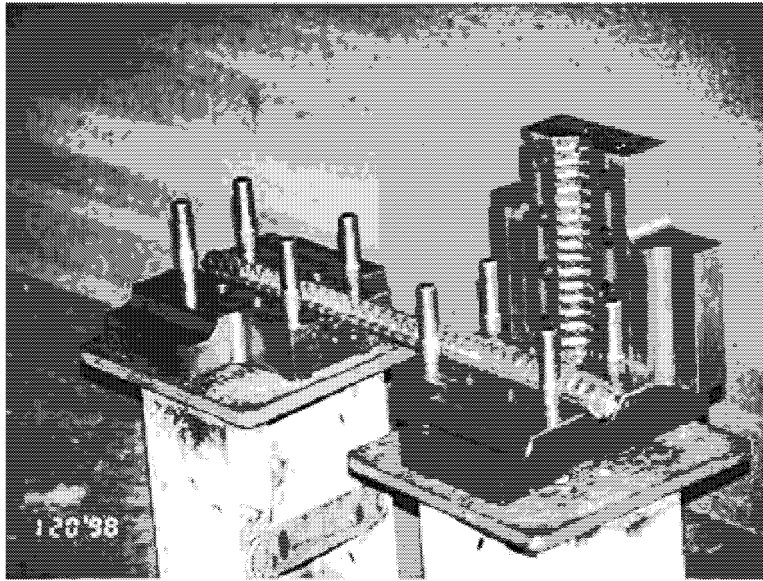


Figure 4-3 Specimen in Grips Ready for Bolting

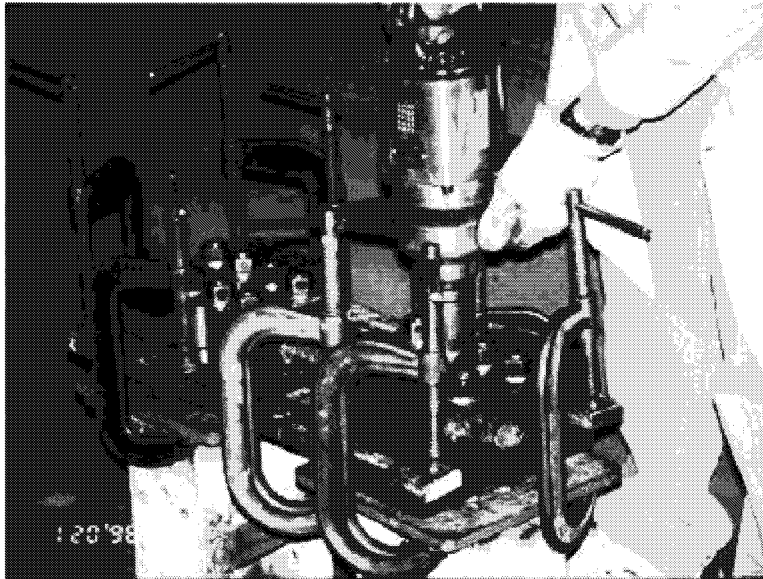


Figure 4-4 Securing Specimen in Rebar Grip

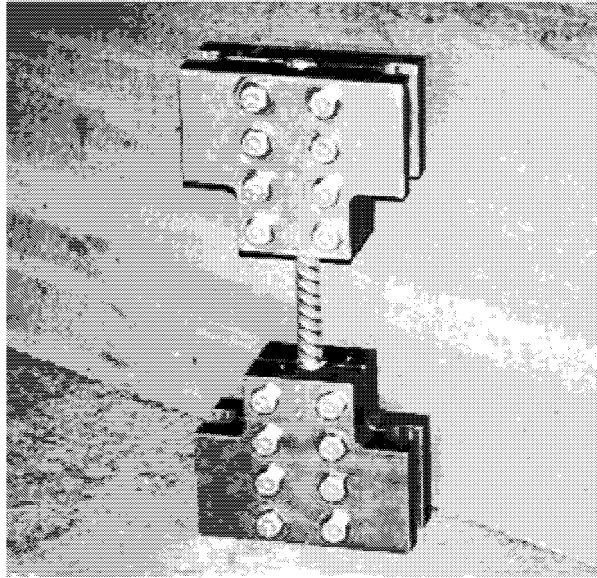


Figure 4-5 Completed Specimen Ready for Testing

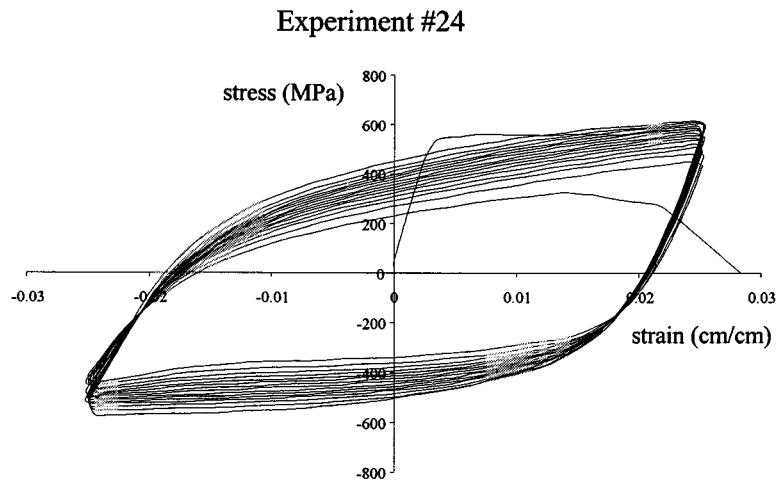


Figure 4-6 Stress vs. Strain data: Experiment #24

A common observation made in all experiments was the formation of multiple fatigue cracks at the base of rolled on deformations. The exact instant of the formation of a fatigue crack was not readily discernable by the naked eye. The stress-strain plots also did not provide any clue on the formation of the first fatigue crack. With the continued application of cyclic deformations,

additional fatigue cracks would develop along the length of the specimen. It is important to note that the presence of a fatigue crack, or even multiple fatigue cracks along the length of the specimen, does not result in immediate failure. While it was often difficult to note the exact cycle in which crack formation occurred, results from these tests indicate that as much as 40-50% of the specimen's total fatigue-life still remains after initial crack formation.

The remainder of this chapter provides essential results from the constant amplitude experiments performed. Complete stress vs. strain data for all experiments are reported in the thesis by Jeff Brown (1996).

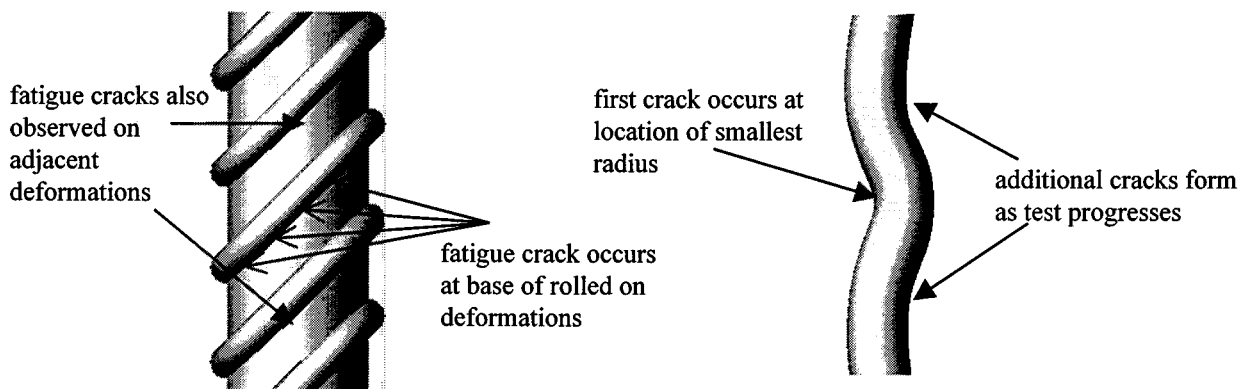


Figure 4-7 Location of Fatigue Crack Formation

#19m Specimens

Table 4-1 #19m Specimens: Constant Amplitude Results

Experiment #	Total Strain Amplitude +/- ϵ_a	Plastic Strain Amplitude +/- ϵ_p	Half Cycles to 1 st Crack N_f	Half Cycles to Failure N_f	Total Energy to Failure W_{fT} (MPa)
21	0.015	0.011	56	87	725.5
22	0.0175	0.0135	31	61	600.1
23	0.02	0.0155	31	49	---
24	0.025	0.0198	17	30	478.9
25	0.03	0.023	9	22	385.8
26	0.0225	0.018	25	44	642.1

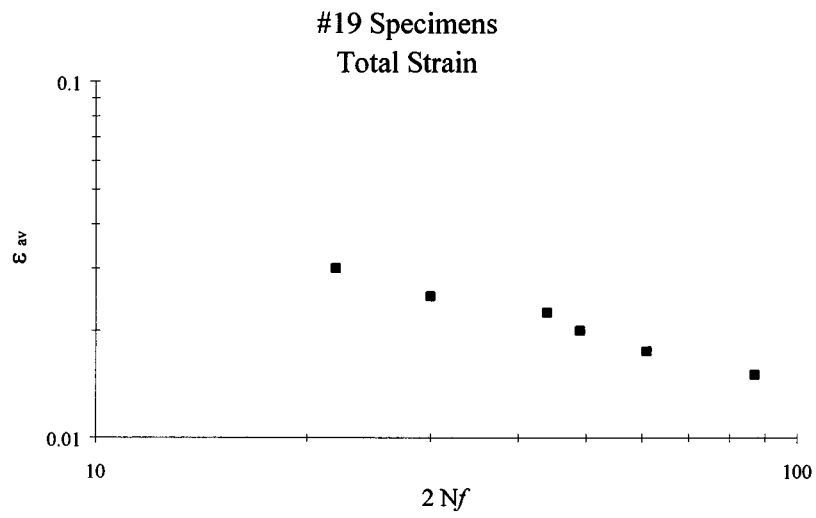


Figure 4-8 Fatigue-life Data (total strain)

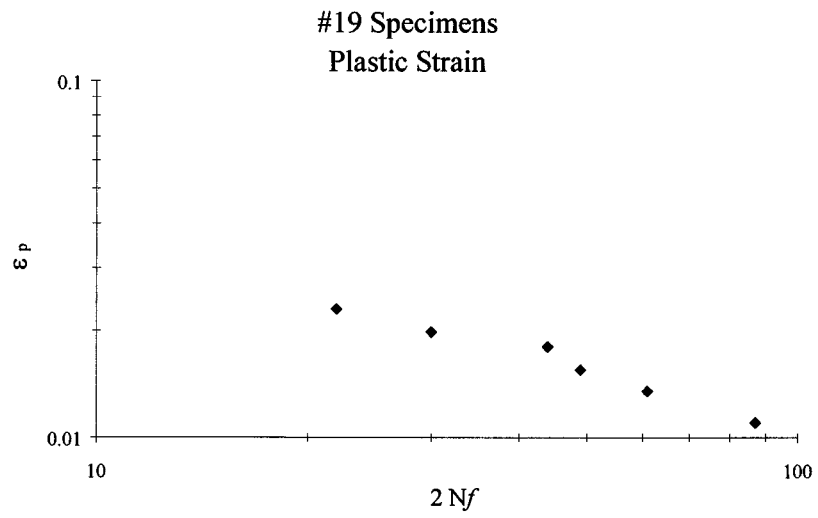


Figure 4-9 Fatigue-life Data (Plastic Strain)

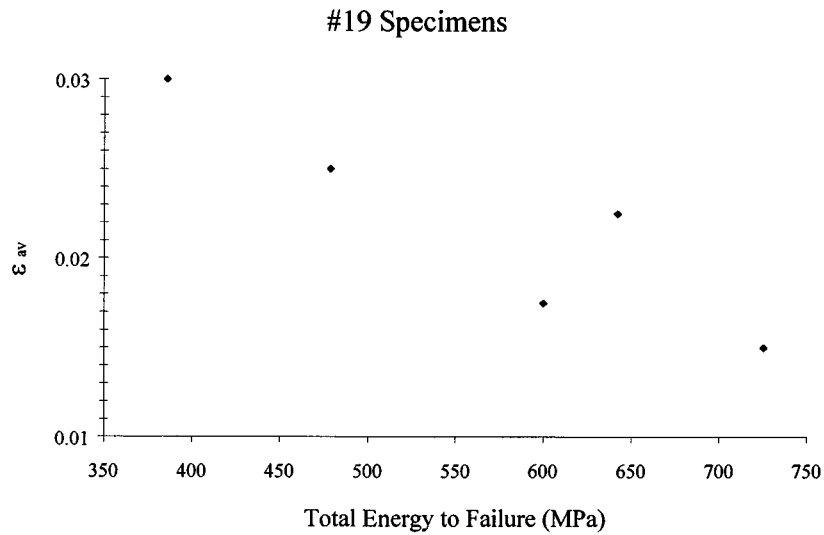


Figure 4-10 Strain Amplitude vs. Total Energy to Failure

#22m Specimens

Table 4-2 #22m Specimens: Constant Amplitude Results

Experiment #	Strain Amplitude $\pm \epsilon_a$	Plastic Strain Amplitude $\pm \epsilon_p$	Half Cycles to 1 st Crack N_f	Half Cycles to Failure N_f	Total Energy to Failure W_{ft} (MPa)
27	0.02	0.0155	23	46	570.3
28	0.0175	0.0135	33	61	608
29	0.0225	0.018	21	42	601.7
30	0.025	0.0198	21	38	655.7
31	0.0275	0.0229	15	22	428.2
32	0.015	0.011	43	92	831.3
33	0.0125	0.0094	87	154	1123
34	0.0175	0.0135	35	95	1011.2
35	0.025	0.0198	22	38	633.8
36	0.03	0.023	10	24	518.8

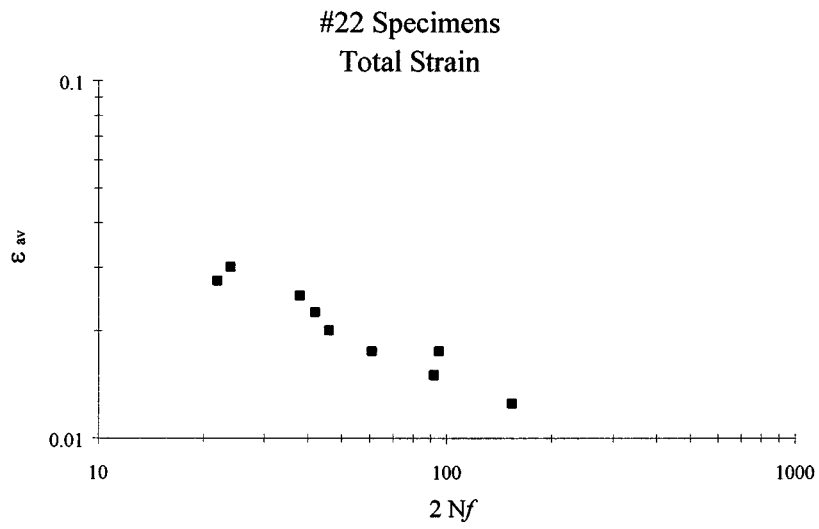


Figure 4-11 Fatigue-life Data (Total Strain)

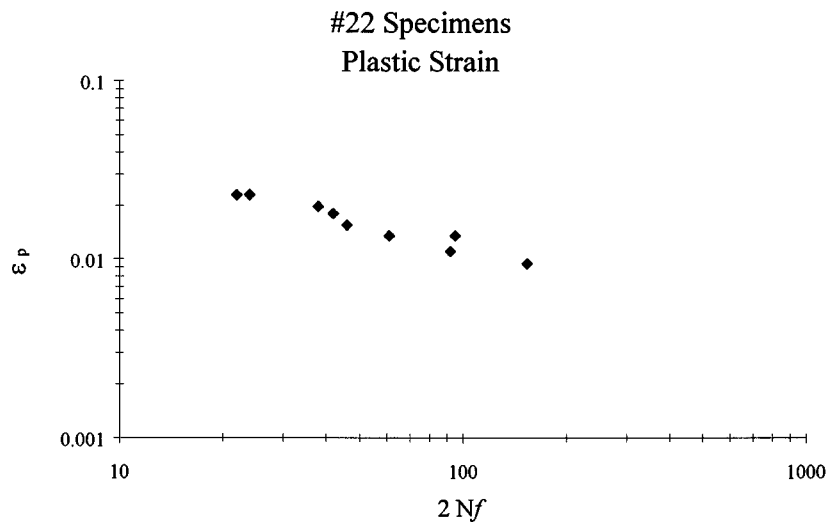


Figure 4-12 Fatigue-life Data (Plastic Strain)

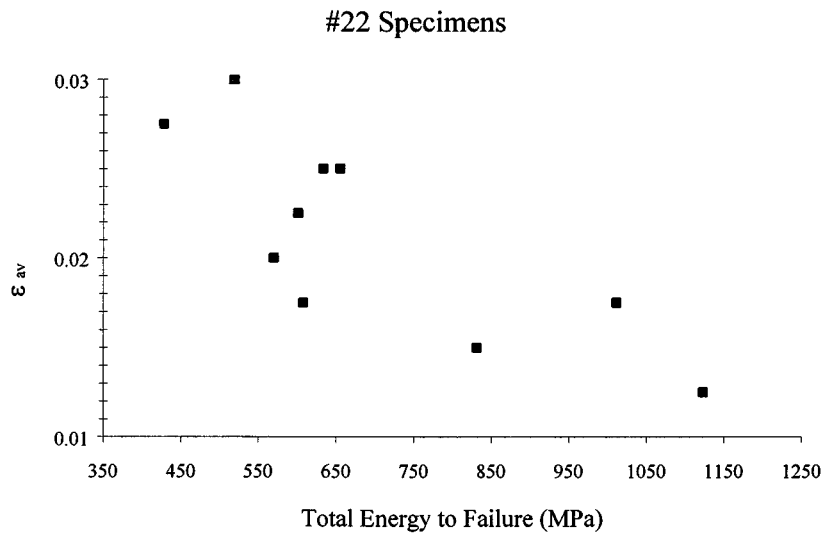


Figure 4-13 Strain Amplitude vs. Total Energy to Failure

#25m Specimens

Table 4-3 #25m Specimens: Constant Amplitude Results

Experiment #	Strain Amplitude $\pm \epsilon_a$	Plastic Strain Amplitude $\pm \epsilon_p$	Half Cycles to 1 st Crack N_f	Half Cycles to Failure N_f	Total Energy to Failure W_{ft} (MPa)
43	0.015	0.011	45	111	962.7
44	0.02	0.0155	33	61	767.6
45	0.025	0.0198	21	28	454.9
46	0.0175	0.0135	21	78	884.4
47	0.0225	0.018	15	44	672.5

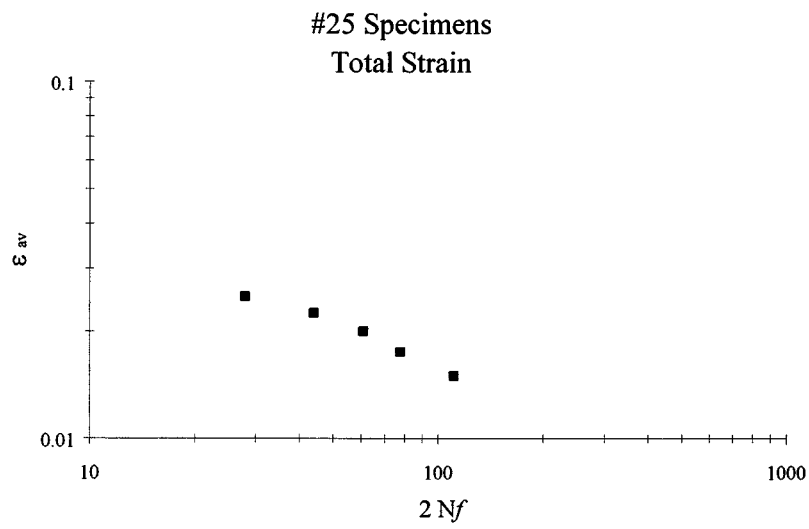


Figure 4-14 Fatigue-life Data (Total Strain)

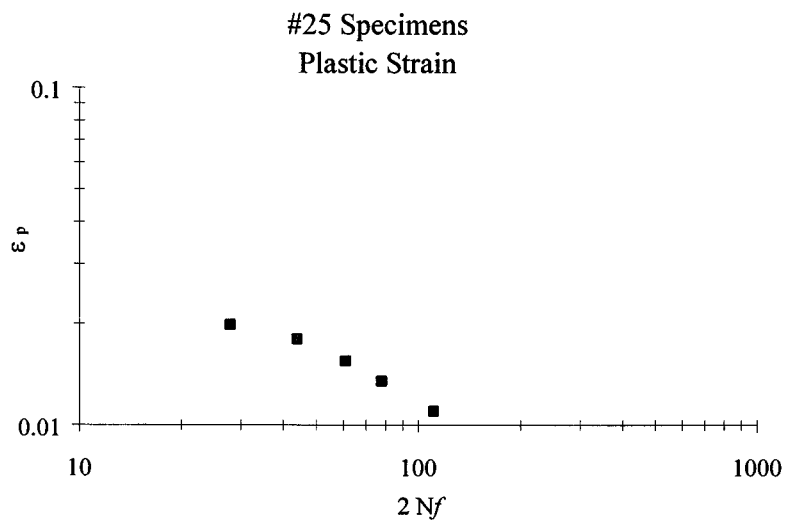


Figure 4-15 Fatigue-life Data (Plastic Strain)

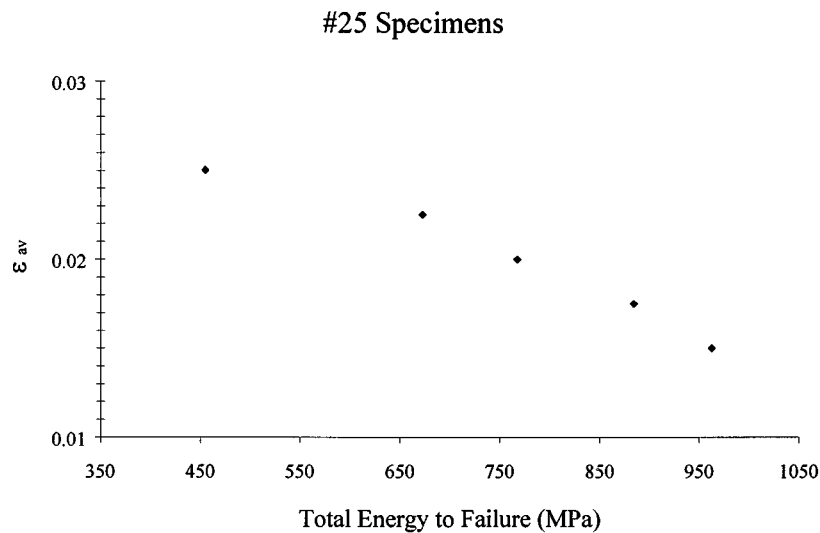


Figure 4-16 Strain Amplitude vs. Total Energy to Failure

4.2 Random Amplitude Testing

In order to investigate the low-cycle fatigue behavior of concrete reinforcement under seismic loading, random amplitude strain history experiments were also performed. These tests could be utilized to calibrate and validate a cumulative damage model that characterizes low cycle fatigue behavior under seismic loading. A brief summary of the random strain histories utilized in the experiments and a summary of the observed results are described in the succeeding sections.

4.2.1 Generation of Random Amplitude Strain Histories

The strain histories used in the present study were chosen to match the random loading histories developed by Kunnath et al (1997) to investigate load path effects in cumulative seismic damage of RC bridge piers. In the study by Kunnath et al., three classes of displacement histories (each class containing several specific histories) were derived from ground acceleration data that were expected to result in varying levels of damage. By assembling event histories from each of the classes in pre-arranged orders to reflect different damage scenarios, load histories for each of the six specimens tested were created. Table 4-4 describes the purpose of each load history class.

More information regarding the procedure and techniques used to determine the random displacement histories is available in Kunnath et al (1997).

Table 4-4 Description of Load History Classes Used for Random Testing

Class	Description
I	Minor earthquake activity not expected to severely damage structural components. Also used to simulate aftershock activity.
II	Moderate to substantial earthquake activity signifying a major event.
II	Severe earthquake expected to result in high levels of damage to structural components. This class of histories was used to ultimately fail each specimen.

The procedure used to test the model columns involved imposing lateral cyclic deformations at the column tip. Before the load history data could be applied in the present study, it was necessary to convert these tip displacements into equivalent strains occurring in the column's plastic hinge region. Paulay and Priestley (1992) have proposed the following relationship for determining plastic curvature resulting from plastic tip displacements (Figure 4-17):

$$\Phi_p = \frac{\Delta_p / (L - 0.5l_p)}{l_p} \quad (4-1)$$

where: Φ_p = plastic curvature
 l_p = plastic hinge length
 Δ_p = plastic tip displacement
 L = length of column

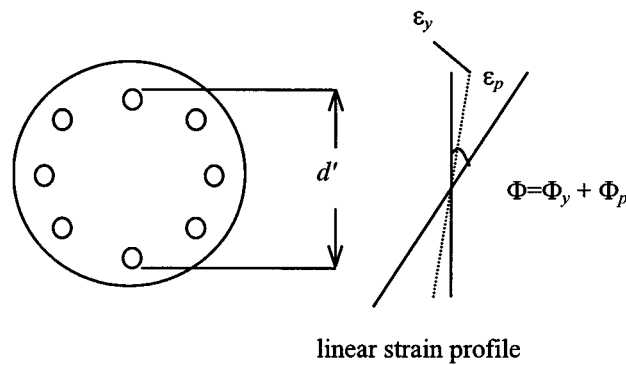


Figure 4-17 Assumed Curvature-Strain Relationship

Once the equivalent plastic curvature has been determined, plastic strains may be obtained with the relationship:

$$\varepsilon_p = \frac{\Phi_p d'}{2} \quad (4-2)$$

where: ε_p = plastic strain

d' = distance between extreme longitudinal rebars

This relationship assumes that depth of the neutral axis remains essentially the same for both forward and reverse cycles, which is reasonable for bridge columns with low levels of axial loads. Further, the computation of plastic strain using the above relationships are approximate. For the purpose of generating random amplitude strain histories, however, it was deemed sufficient. In order to implement each strain history into the hydraulic control routine, it was necessary to eliminate strain cycles with peak to peak magnitudes less than .001. This limitation was a result of the actuator's inability to produce sufficiently small displacements without overshooting the target. Table 4-5 summarizes the actual strain histories used in the random amplitude tests. The table also shows the total energy dissipated prior to fracture of the specimen. The number of cycles to failure varied from one experiment to another because of the random nature of the imposed history. Additional discussion on random amplitude tests and converting random cycles into equivalent constant amplitude cycles is presented in the next section.

Table 4-5 Imposed Strain Histories for Random Amplitude Experiments

Experiment (bar size)	Loading History Case Sequence	Earthquake Record	Total Energy to Failure	Strain History
37 (22)	II I I III (1 - 1)*	<ol style="list-style-type: none"> 1. Loma Prieta 1989 (Presidio) 2. Imperial Valley 1979 (Superstition Mountain) 3. San Fernando 1971 (2011 Zonal Ave.) 4. San Fernando 1971 (455 S. Figueroa) 	452.8	
38 (22)	I I II III (1 - 3)	<ol style="list-style-type: none"> 1. Imperial Valley 1979 (Superstition Mountain) 2. San Fernando 1971 (2011 Zonal Ave.) 3. Loma Prieta 1989 (Presidio) 4. San Fernando 1971 (455 S. Figueroa) 	689.4	
39 (22)	II I II I III (1 - 4)	<ol style="list-style-type: none"> 1. San Fernando 1971 (Orion Blvd.) 2. San Fernando 1971 (2011 Zonal Ave.) 3. El Centro 1940 4. San Fernando 1971 (455 S. Figueroa) 5. San Fernando 1971 (Orion Blvd.) 	563.8	
40 (22)	I II I II III (1 - 5)	random history #4	500.3	
41 (22)	II I I III (2 - 4)	random history #5	662.4	

Table 4-5 (continued) Imposed Strain Histories for Random Amplitude Experiments

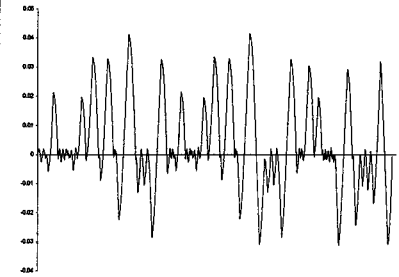
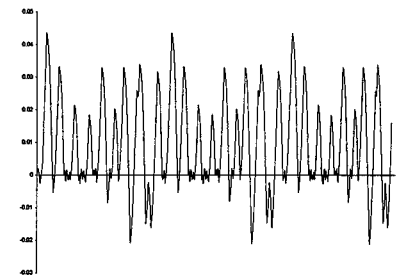
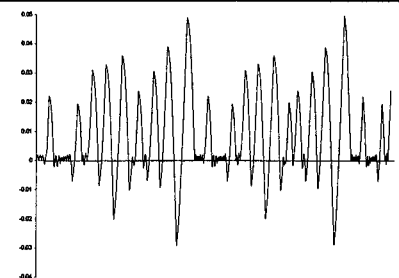
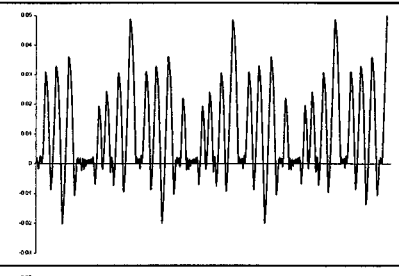
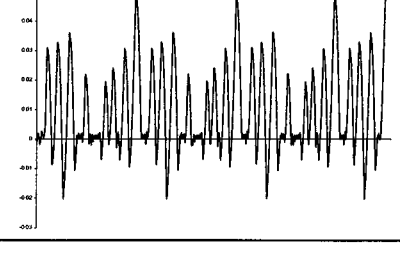
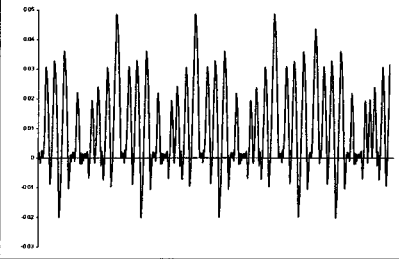
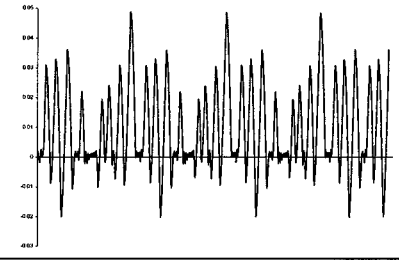
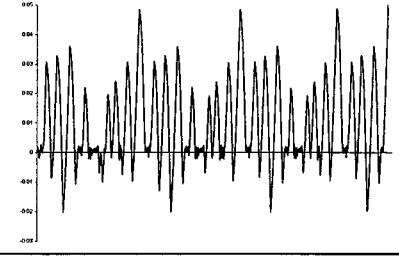
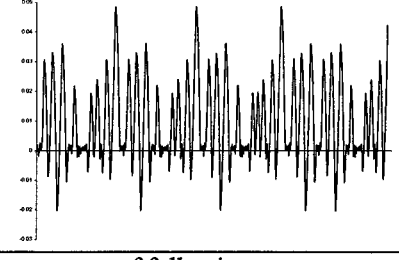
Experiment (bar size)	Loading History Case Sequence	Earthquake Record	Total Energy to Failure (MPa)	Strain History
42 (22)	I I II III (2 - 1)	random history #6	507.9	
48 (25)	II I I III (2 - 4)	random history #1	600	
49 (25)	I II I II III (2 - 2)	random history #4	520.1	
50 (25)	II I II I III (3 - 2)	random history #3	695.9	
51 (25)	II I II I III (3 - 2)	random history #3	711.4	

Table 4-5 (continued) Imposed Strain Histories for Random Amplitude Experiments

Experiment (bar size)	Loading History Case Sequence	Earthquake Record	Total Energy to Failure (MPa)	Strain History
52 (25)	I II I II III (3 - 5)	random history #7	806.3	
53 (25)	II I II I III (3 - 4)	random history #3	686.0	
54 (25)	II I II I III (3 - 2)	random history #3	625.4	
55 (25)	I II I II III (3 - 5)	random history #7	813.0	

** $(n - m)$ indicates specimen survived n full sequences and failed during event m of following sequence

4.3 Observations

Figure 4-18 provides stress vs. strain data obtained from experiment #48. Fatigue crack and failure patterns were similar to those encountered during the constant amplitude experiments. Several fatigue cracks along the specimen's length would develop at the base of rolled on deformations roughly half way through each experiment. Each crack would continue to propagate throughout the remainder of the experiment until rupture finally occurred. Prior to the

last one or two cycles, it was not possible to recognize exactly which crack would result in rupture. This indicates that, even after crack formation, the entire length of the specimen is absorbing deformations.

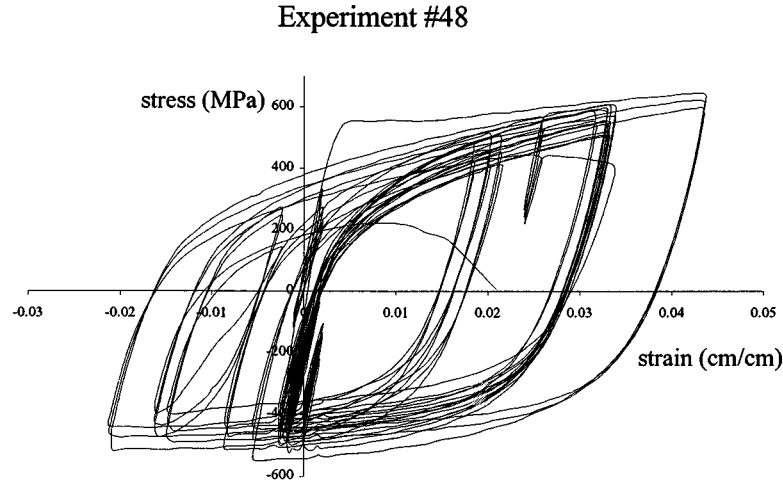


Figure 4-18 Stress vs. Strain Data: Experiment #48

A particularly interesting observation made during these experiments was related to the behavior of the buckled profile. In the constant amplitude tests, the specimen's buckled profile varied from perfectly straight to severe in tension and compression, respectively. In the random amplitude tests, however, it was common for large tension cycles to permanently increase the length of the specimen. When the following compression cycle was experienced, a new buckled profile would result. Until the specimen was subjected to a tension cycle of near equal or greater magnitude than the previous maximum, there was a tendency for the buckled profile to remain during smaller tension cycles. This observation is illustrated in Figures 4-19 and 4-20, which show a slight buckled profile remaining just prior to and after tension rupture.

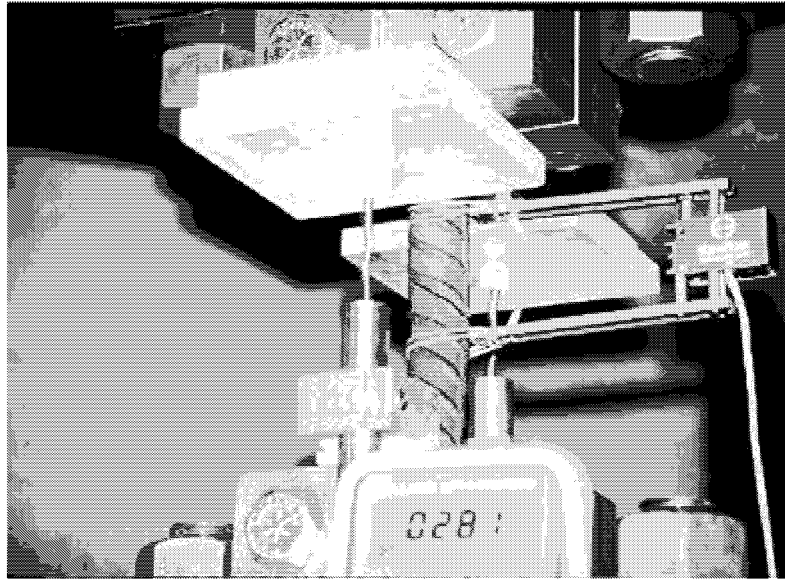


Figure 4-19 Fatigue Crack Just Prior to Failure (Experiment #48)

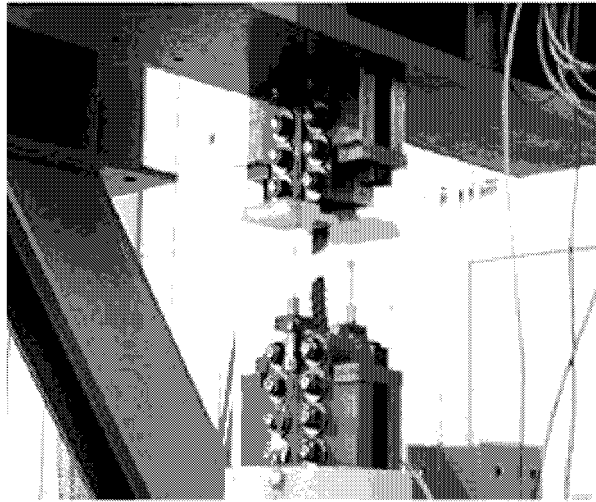


Figure 4-20 Final State of Specimen After Rupture

4.4 Summary

Results of fatigue testing on three different rebar sizes under both constant-amplitude loading and variable amplitude loading were summarized in this section. Constant-amplitude tests consisted of reversed cyclic strains in the range of 0.015 to 0.03. The strain histories for the random-amplitude tests were determined from analytically estimated rebar strains in the plastic hinge region of a flexural bridge column subjected to a series of earthquake loads. Fatigue life was defined in two ways: (1) the occurrence of the first crack as determined by visual observation; and (2) the rupture of the rebar. In addition to calibrating the number of half-cycles to failure, the total strain energy was also established for each rebar size.

SECTION 5

ANALYSIS OF RESULTS, OBSERVATIONS AND SIGNIFICANT FINDINGS

In this section of the report, existing fatigue models are applied to the constant amplitude fatigue experiments and these relationships are extended to address random loading histories. Issues regarding cycle counting techniques will also be examined. Finally, results of these experiments will be compared to those of Mander et al (1994).

5.1 Fatigue-life Models

The objective of a fatigue-life model is to predict the failure of a material or component subjected to cyclic loading. By examining quantities such as total strain amplitude, plastic strain amplitude, absorbed energy, and number of cycles to failure from experimental data, observed trends become the foundation for such models. In general, fatigue-life models for constant amplitude experiments take the following form:

$$y = a (x)^c \tag{5-1}$$

where: y = deformation quantity
 x = number of half or full cycles to failure
 a and c = constants derived from experimental data

When plotted on a log-log scale, the above relationship becomes linear. This is a commonly observed phenomenon in fatigue-life testing. As seen in the plots presented in Chapter 4, the data collected during these experiments also follows this trend. Each of the following subsections will document the application of various existing fatigue-life models. This will provide the necessary calibration constants required for the analysis of random load histories.

5.1.1 Total Strain Amplitude

Koh and Stephens (1991) proposed the following fatigue-life model used to relate total strain amplitude to the corresponding number of half cycles (or strain reversals) to failure:

$$\varepsilon_a = \frac{\Delta\varepsilon}{2} = M(2N_f)^m \quad (5-2)$$

where: ε_a = total strain amplitude

$\Delta\varepsilon$ = total strain range ($\varepsilon_{\max} - \varepsilon_{\min}$)

M and m = material constants

$2N_f$ = number of half cycles to failure

It is important to establish precisely the definitions of the variables used in the above equation. Consider the simple constant amplitude strain history shown in Figure 5-1. In this case, the total number of half cycles to failure is four. This is the result of having been subjected to cyclic deformations at a constant level of $\pm \varepsilon_a$. For random load histories, the equation is easier to implement in terms of $\Delta\varepsilon$ since this quantity represents the total strain range experienced during a single half cycle.

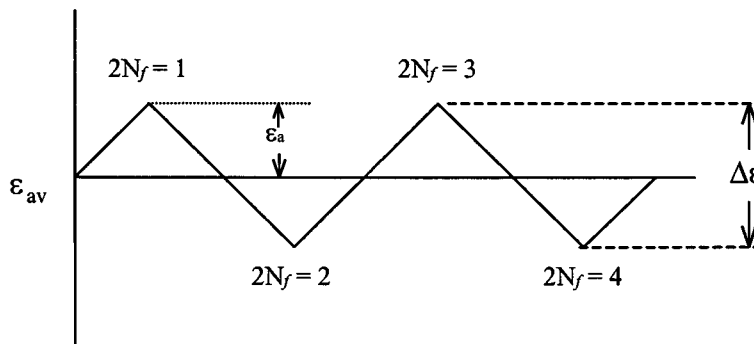


Figure 5-1 Simple Constant Amplitude Strain History

Curve fit data for all three bar sizes tested is presented in Figure 5-2. Resulting fatigue-life curves generated for each bar size are very similar, and a fatigue-life curve obtained by

combining results from all of the constant amplitude experiments fits the data very well. Without additional testing to create a statistically valid database of fatigue-life data, any conclusion regarding bar size effects may be premature. From the data collected, however, the following general trend was observed: At high deformation amplitudes, smaller bar sizes exhibit a slightly higher resistance to fatigue failure. At relatively low levels of deformation amplitude (high number of cycles to failure), larger bar sizes offer better resistance. This trend may also be a result of the rolled on deformation geometry in combination with the specimen's cross-sectional area.

Another fatigue model involving total strain amplitude was also considered. This model, again proposed by Koh and Stephens, includes the effect of strength degradation by considering the stress developed at the tension peak corresponding to the specimen's half-life. The following expression summarizes this relationship:

$$\varepsilon_a f_{mx} = C(2N_f)^\gamma \quad (5-3)$$

where: f_{mx} = maximum tensile stress at the half-life of each specimen

C and γ = material constants

Figure 5-3 presents fatigue-life curves that appear very similar to those shown previously. The only major difference is that the y-axis is scaled by the corresponding maximum tensile stress achieved at the specimen's half-life. It is difficult to draw certain conclusions about the value of stress obtained at the specimen's half-life since both strain hardening and strength degradation effect this number simultaneously.

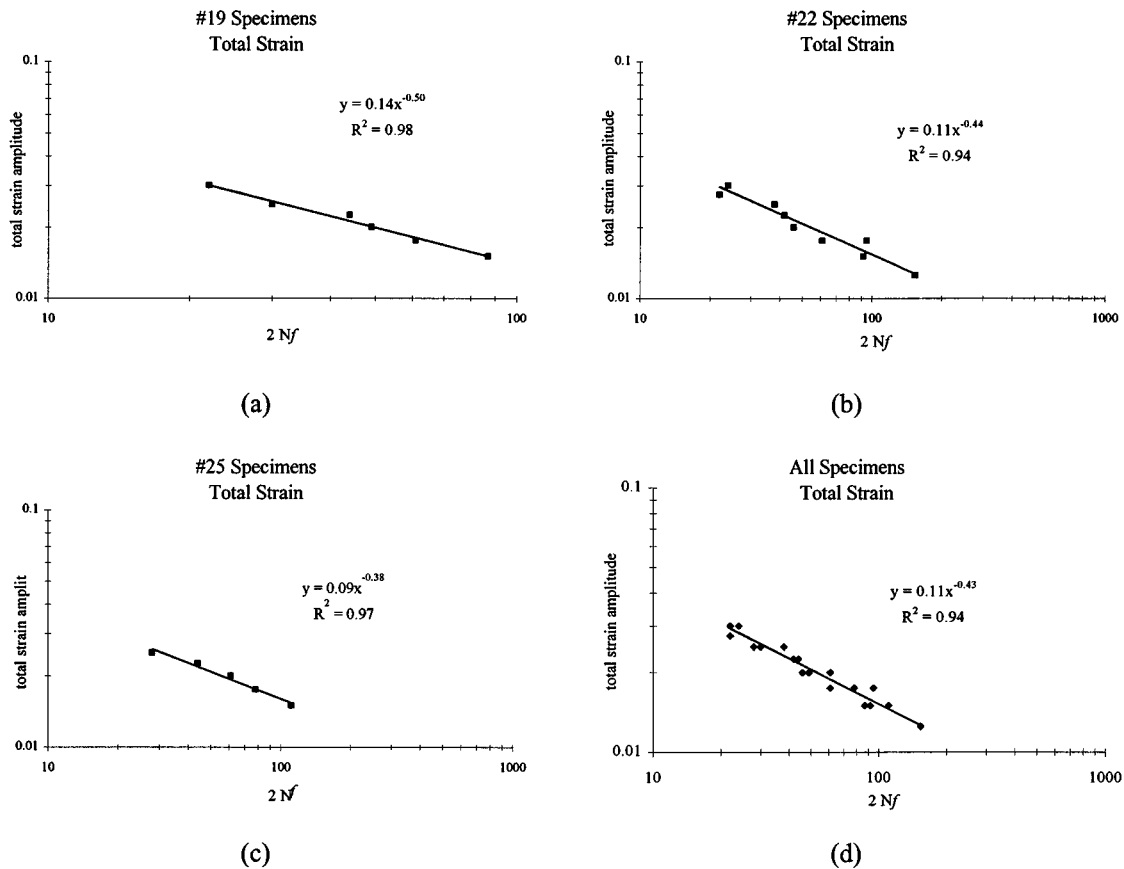


Figure 5-2 Fatigue-life Curves Considering Total Strain Amplitude

5.1.2 Plastic Strain Amplitude

When considering low-cycle fatigue, it is often common to focus only on the plastic strain experienced by the specimen. The original Coffin-Manson equation (1953-54) was of this sort and served as the basis for many subsequent fatigue-life models. Figure 5-4 illustrates the difference in plastic strain amplitude, $\Delta\epsilon_p$, and total strain amplitude, $\Delta\epsilon$.

Lorenzo and Laird (1984) also proposed a modification to the Coffin-Manson equation that includes the effects of maximum stress at each specimen's half-life. Fatigue-life curves and resulting curve fit equations are presented for each bar size tested in Table 5-3.

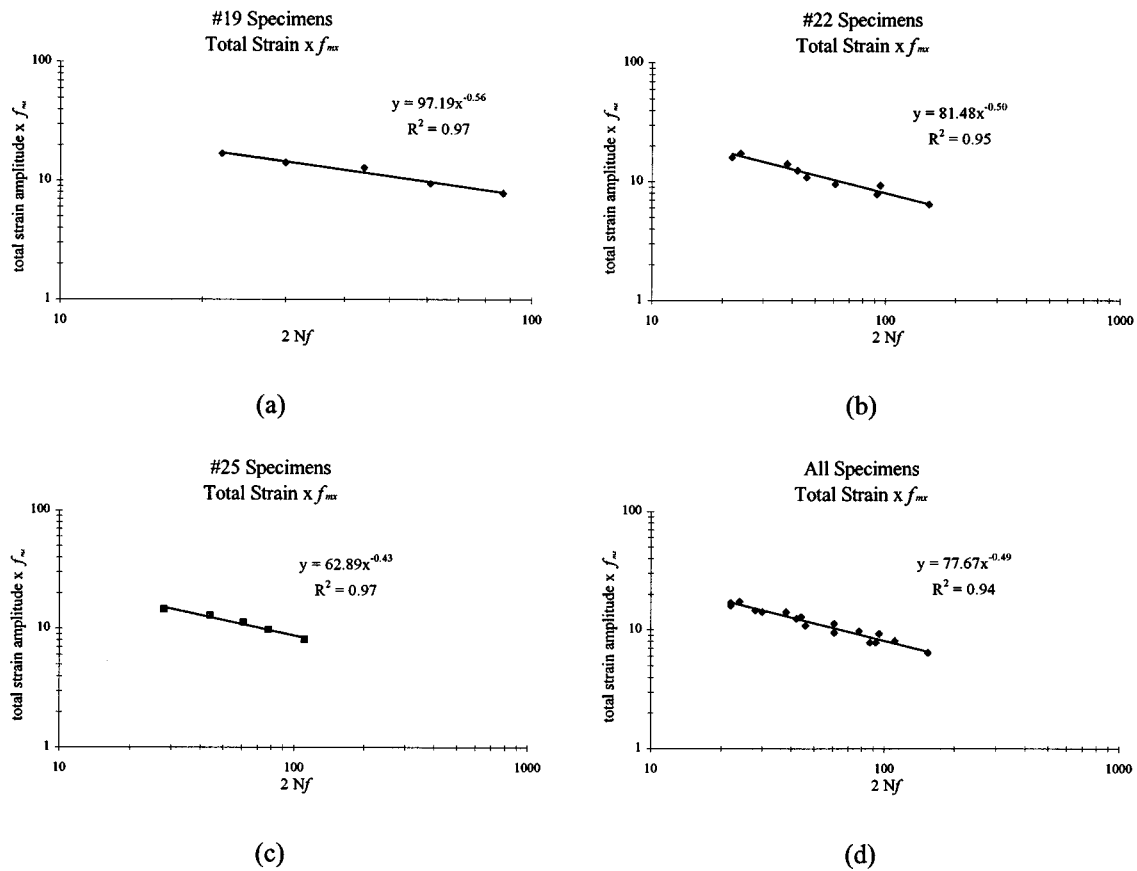


Figure 5-3 Fatigue-life Curves Modified for Max Stress at Specimen Half-Life

Table 5-1 Summary of Fatigue-life Curves: Koh and Stephens' Model for Total Strain

Bar Size	Curve Fit	r^2
19	$\epsilon_a = 0.142(2Nf)^{-0.503}$.984
22	$\epsilon_a = 0.115(2Nf)^{-0.437}$.937
25	$\epsilon_a = 0.091(2Nf)^{-0.377}$.975
all tested	$\epsilon_a = 0.112(2Nf)^{-0.433}$.941

Table 5-2 Summary of Fatigue-life Curves: Koh and Stephens' Modified for Strength

Bar Size	Curve Fit	r^2
19	$f_{mx} \epsilon_a = 97.19(2Nf)^{-.560}$.974
22	$f_{mx} \epsilon_a = 81.48(2Nf)^{-.503}$.945
25	$f_{mx} \epsilon_a = 62.89(2Nf)^{-.428}$.974
all tested	$f_{mx} \epsilon_a = 77.67(2Nf)^{-.490}$.939

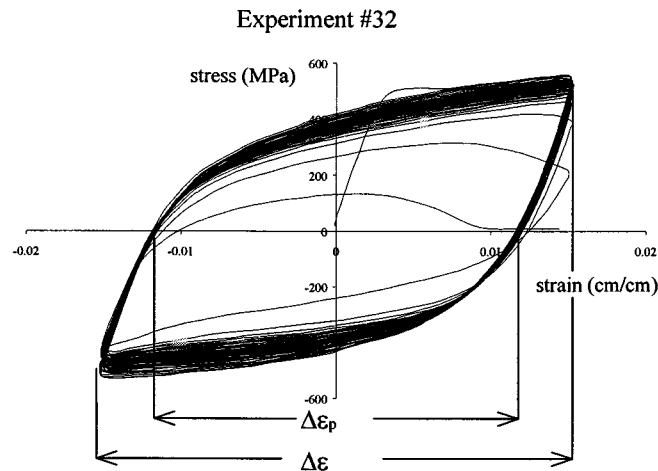


Figure 5-4 Plastic Strain Amplitude, $\Delta\epsilon_p$

Table 5-3 Summary of Fatigue-life Curves: Coffin-Manson Model for Plastic Strain

Bar Size	Curve Fit	r^2
19	$\epsilon_{ap} = 0.124(2Nf)^{-.536}$.968
22	$\epsilon_{ap} = 0.105(2Nf)^{-.478}$.939
25	$\epsilon_{ap} = 0.088(2Nf)^{-.432}$.960
all tested	$\epsilon_{ap} = 0.102(2Nf)^{-.473}$.938

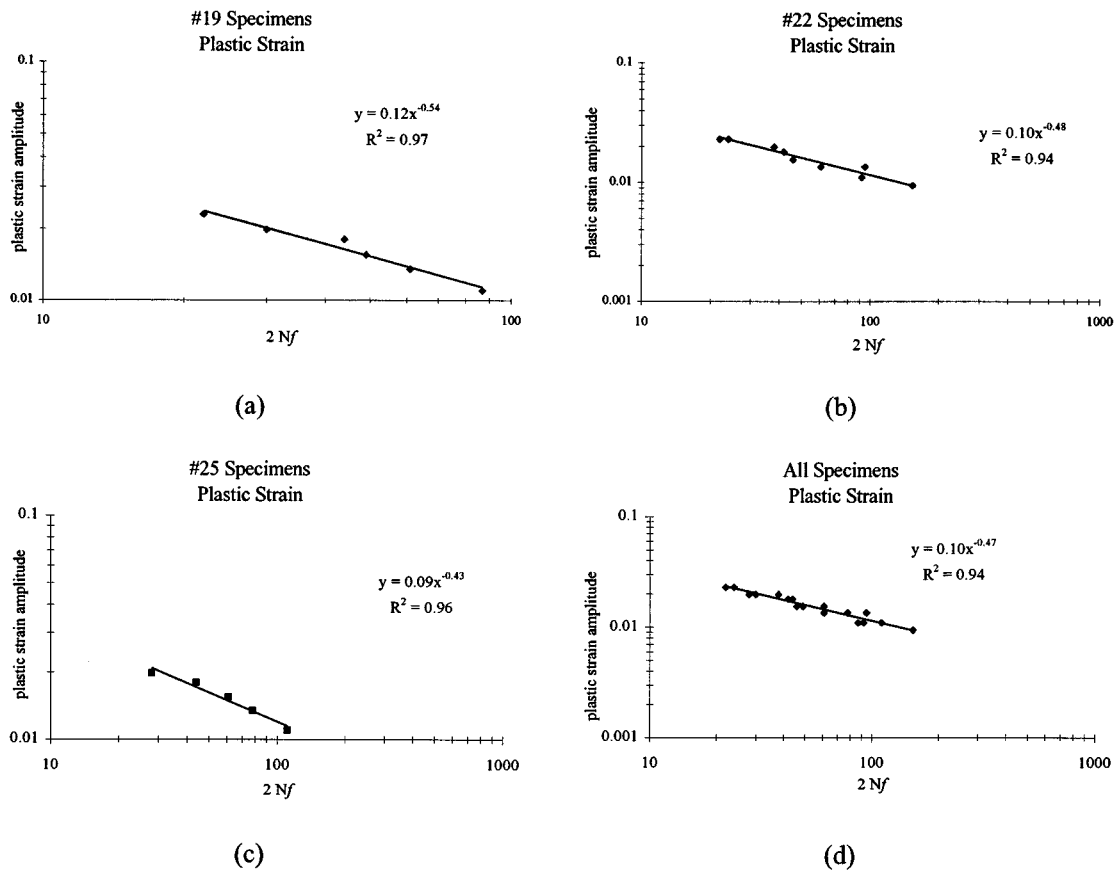


Figure 5-5 Fatigue-life Curves Considering Plastic Strain Amplitude

Table 5-4 Summary of Fatigue-life Curves: Lorenzo and Laird Modified for Strength

Bar Size	Curve Fit	r^2
19	$f_{mx} \epsilon_{ap} = 85.20(2Nf)^{-0.594}$.953
22	$f_{mx} \epsilon_{ap} = 74.33(2Nf)^{-0.543}$.946
25	$f_{mx} \epsilon_{ap} = 60.62(2Nf)^{-0.483}$.960
all tested	$f_{mx} \epsilon_{ap} = 70.50(2Nf)^{-0.530}$.933

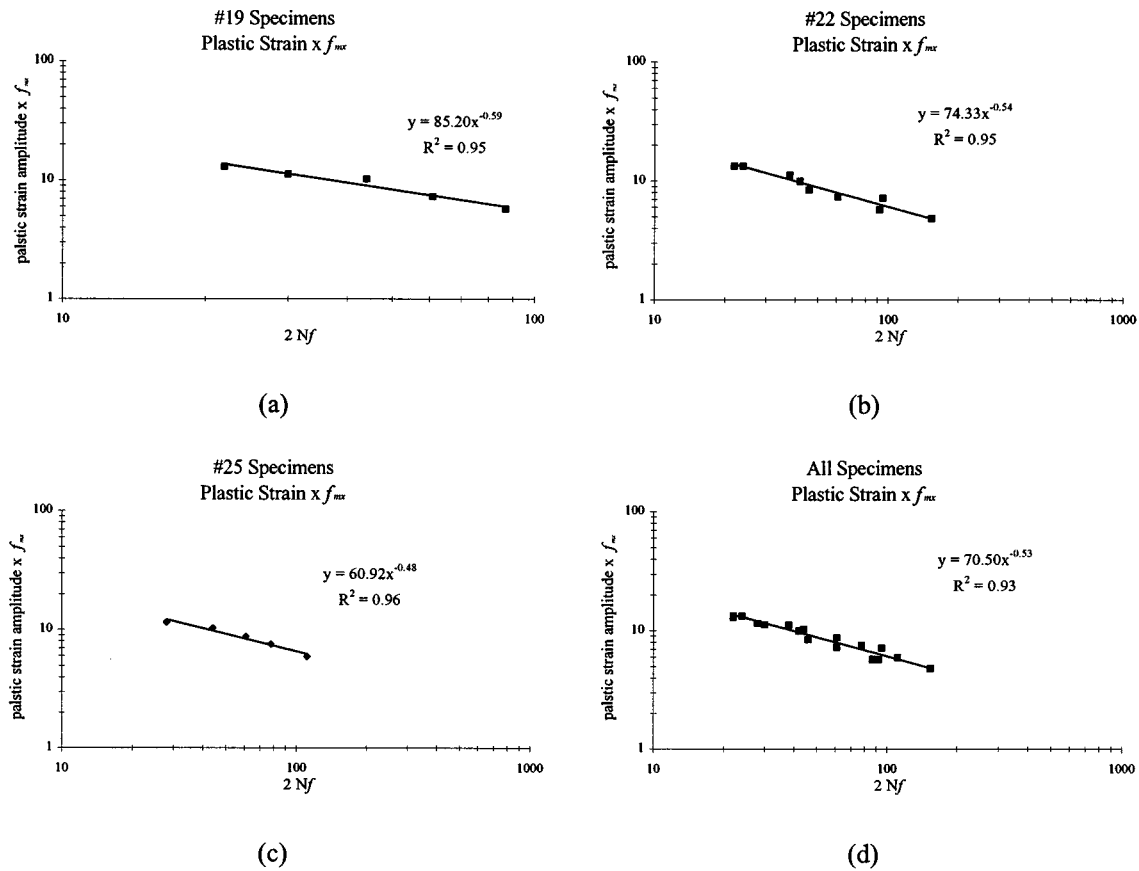


Figure 5-6 Plastic Strain FLCs Modified for Max Stress at Specimen Half-Life

The data collected during these constant amplitude experiments appears to follow very closely the trends established in existing fatigue-life models. The experiments were useful in obtaining the material specific quantities that each model requires. Unfortunately, there is insufficient data present to draw any firm conclusions regarding the effect of bar size. With reference to equation 5-1, the a and c terms present both tend to decrease as the bar size increases. Including all specimens in the curve fit process yields a result most closely related to the #22 specimens. This is most likely a result of the non-proportional quantity of data associated with these specimens. Overall, however, the curve fit obtained from including all specimens tested appears to provide an acceptable relationship between number of half cycles to failure and deformation amplitude for all bar sizes (#19-#25).

The fatigue-life models containing provisions for the maximum stress experienced at the specimen's half-life differ very little from those considering only deformation amplitude. This is to be expected since the maximum stress experienced will not vary considerably after yielding. The original formulation was intended to include the effects of mean stress, presumably in the high cycle fatigue range. Curve fit data was provided for the purpose of comparison with previous work and will not be utilized in the analysis of random load histories.

5.1.3 Energy Based Formulations

Mander et al (1994) proposed several fatigue-life models that relate total energy absorbed by the specimen and deformation amplitude. This particular quantity is obtained by numerically integrating the stress vs. strain data collected during each experiment. Similar to the fatigue-life models discussed previously, deformation quantities are described in terms of total strain amplitude, plastic strain amplitude, and a product of each quantity with the maximum stress achieved by the specimen during each experiment. Details of these four models were presented in Section 1.

Total strain amplitude vs. energy to failure is plotted in Figure 5-7 for all specimens tested. There is certainly an observed trend; however, the correlation is not as well defined as with the previous fatigue-life models. As the total deformation amplitude decreases, there is an increase in the energy absorption capacity of the specimen. Even though the quantity of energy absorbed during each cycle is greater for larger deformation amplitudes, the damage incurred reduces a specimen's energy capacity at a rate faster than that of smaller deformations. Curve fit data for these models is provided in Table 5-5.

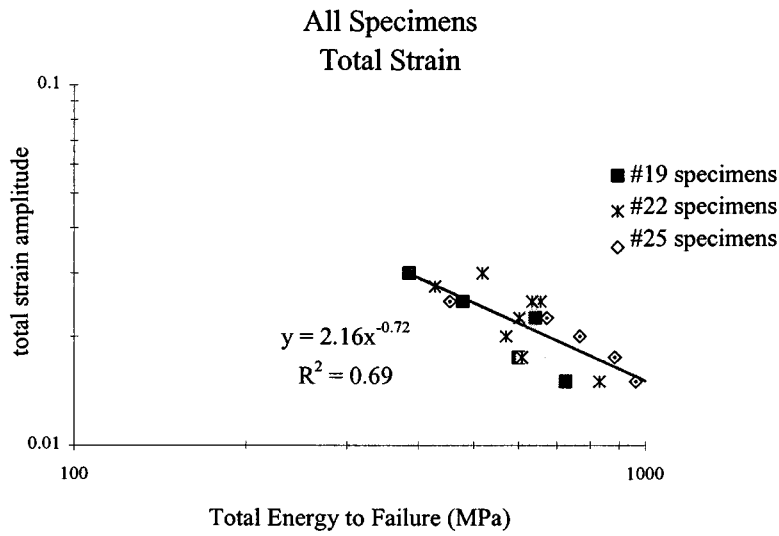


Figure 5-7 Total Strain Amplitude vs. Energy to Failure

Table 5-5 Curve Fit Data for Energy Based Models Proposed by Mander et al (1994)

Model	Curve Fit	r^2
Energy - (total strain)	$W_{fT} = 2.16(\epsilon_a)^{-0.718}$.688
Energy - (plastic strain)	$W_{fT} = 2.50(\epsilon_{ap})^{-0.781}$.678
Energy - (stress X total strain)	$W_{fT} = 2123.5(f_{max} \epsilon_a)^{-0.808}$.677
Energy - (stress X plastic strain)	$W_{fT} = 2461.7(f_{max} \epsilon_{ap})^{-0.870}$.667

5.2 Observations on Stress vs. Strain Behavior

Another phenomenon that can also be attributed to fatigue is strength degradation. As the specimen repeatedly deforms to its maximum level of deformation, the corresponding stress at subsequent cycles will be different. This is a very important concept in the global modeling of RC columns since a loss of strength in a column's reinforcement will tend to alter its moment-

curvature (hysteresis) behavior under cyclic loading. These experiments offered an excellent opportunity to monitor strength decay and relate this quantity to the specimens' deformation amplitude.

A convenient way to monitor strength decay is by normalizing all peak stresses recorded for each cycle, f_i , with respect to the stress achieved at the first peak, f_0 . Tension and compression peaks are treated separately to better observe the trend in each. Figure 5-8 provides a plot for select #19 specimens of f_i / f_0 vs. number of full cycles to failure at each tension peak. The first few cycles in every experiment possess f_i / f_0 ratios greater than 1 as a result of strain hardening. The maximum ratio achieved is a function of the level of imposed deformations. Larger strain amplitude cycles will result in higher degrees of strain hardening. After the peak ratio has been obtained (near the second or third cycle), the f_i / f_0 ratio begins to decline, the rate of which is, again, dependant upon the level of imposed deformation. Larger strain amplitude cycles will lead to a higher rate of strength decay.

Figure 5-9 shows a similar plot for compression peaks. Unlike the tension peaks, no strain hardening is visible and strength decay begins immediately. The rate of decay is observed to be a function of the deformation amplitude and remains essentially constant up to specimen failure.

What is most interesting to note about both tension and compression peaks is that soon after a f_i / f_0 ratio of approximately 0.75 is reached, the rate of strength decay increases dramatically and is followed closely by failure. This trend does not seem to be affected by deformation amplitude and was observed in the majority of experiments. f_i / f_0 data for each experiment is located in the appendix.

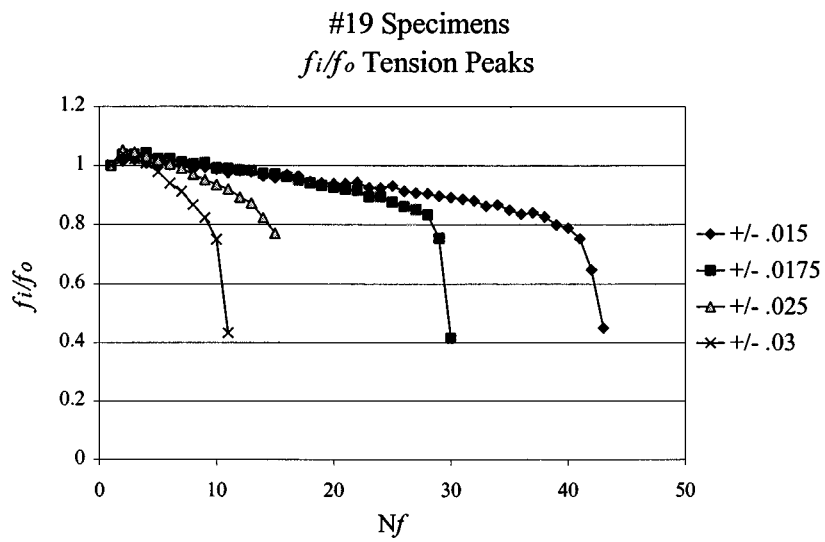


Figure 5-8 f_i/f_o vs. Nf for Different Strain Amplitudes (Tension Peaks)

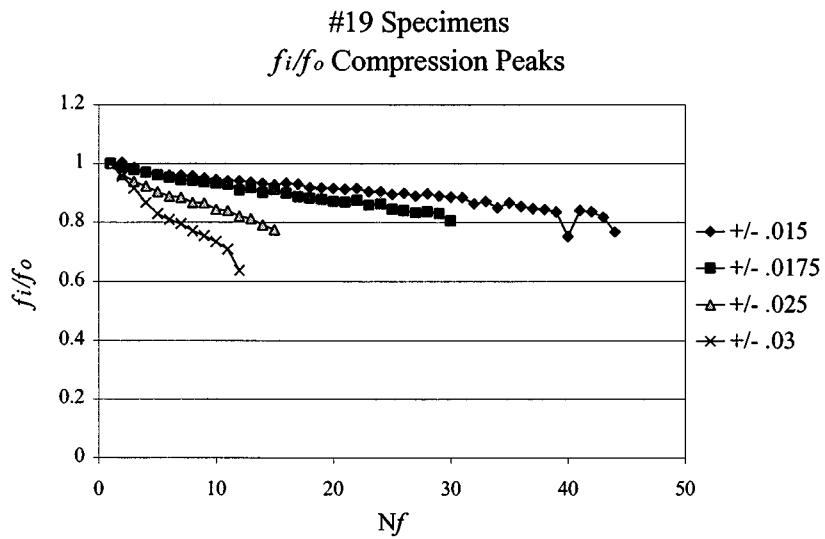


Figure 5-9 f_i/f_o vs. Nf for Different Strain Amplitudes (Compression Peaks)

5.3 Random Amplitude Strain History Analysis

Data collected during the constant amplitude experiments provided a relationship between deformation amplitude and number of cycles to failure. The objective of this section is to apply this relationship, in combination with an appropriate cycle counting technique, in an attempt to predict failure under random cyclic loading.

Miner (1945) proposed a simple model that assumes a linear accumulation of damage as a function of the number of cycles experienced at a specific deformation amplitude:

$$D_{(i)} = \frac{1}{2N_{f(i)}} \quad (5-4)$$

$$D = \sum D_{(i)} \quad (5-5)$$

where: D = damage index

$D_{(i)}$ = resulting damage from one half cycle at deformation $\varepsilon_{(i)}$

$2N_{f(i)}$ = number of half cycles to failure at deformation level $\varepsilon_{(i)}$

In a constant amplitude experiment, failure is always indicated by a damage index equivalent to one. For random load histories the same is expected to be true; however, since this model does not take into account sequence effects, computed damage indices often differ. By applying this linear accumulation rule to the data collected in the random deformation history experiments, conclusions regarding its applicability may be formed.

5.3.1 Rainflow Cycle Counting Method

For random strain histories in which there are relatively few cycles to failure and the majority of damage is attributed to large strain reversal, the rainflow cycle counting is most commonly employed (Suidan and Eubanks, 1973). The objective of this method is to identify strain ranges in a random history such that fatigue-life curve data may be used in the computation of Miner's damage index.

If the random load history is rotated 90 degrees (as shown in Figure 5-10), the resulting profile resembles a series of pagoda style roofs. By carefully monitoring the behavior of a fictitious rainfall (hence the name) as it flows down the series of roofs, equivalent full and half cycles are determined. Rules governing the flow of rain are somewhat difficult to verbalize; however, combined with an example, the method becomes clear. A new water source begins to flow down the roof at every peak. Flow from each source will continue until: (a) it falls from a roof and does not land on a roof below; (b) water falling from a peak crosses a stream flowing in the same direction that originated at a peak of larger opposite magnitude than the flow being terminated; or (c) water running down a roof is met by water falling from a higher roof.

Consider the random strain history shown in Figure 5-10. Flow begins at A and falls off the roof at B. This flow is terminated at B, representing one half cycle of magnitude A-B, since it would fall onto a stream originating at C (of larger opposite magnitude than A). Flow beginning at B would stop at C due to a similar situation with the stopping flow originating at D. Water flowing from C to D, E to F, G to H, and I to J all represent half cycles terminated due to either intercepting flow originating at a peak of larger opposite magnitude or not falling on any roofs below. Flow originating at F, H, and J is stopped as soon as it intercepts flow falling from E, G, and I, respectively.

Table 5-6 provides a summary of the resulting strain ranges when this method is applied to the sample random strain history. The algorithm was implemented in a simple C++ computer program for use with the actual strain histories.

5.3.2 Calculated Damage Indices

After applying the rainflow cycle counting method to the random strain histories, it is possible to compute a resulting damage index based on the constant amplitude experimental results. Recall that for a given strain range:

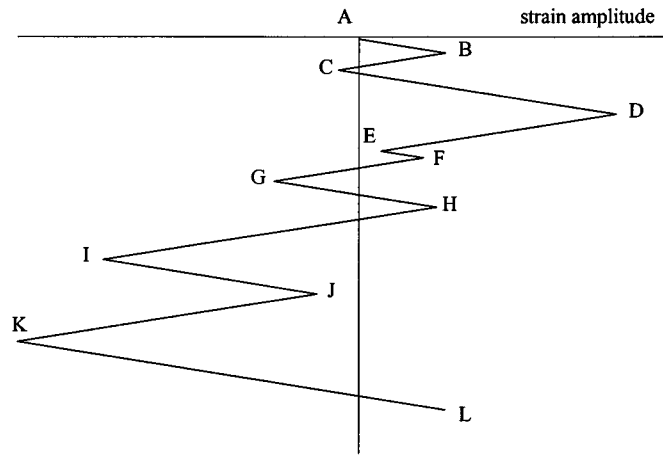


Figure 5-10 Sample random load history to demonstrate rainfall counting method

Table 5-6 Resulting Deformation Ranges from Sample Strain History

Strain Range $\Delta\varepsilon$	Number of Half Cycles
A-B	1
B-C	1
C-D	1
D-K	1
E-F	2
G-H	2
I-J	2
K-L	1

$$\frac{\Delta\varepsilon}{2} = a(2N_f)^c \quad (5-6)$$

Rearranging and solving for $2N_f$:

$$2N_f = \frac{\Delta\varepsilon^{1/c}}{(2a)^{1/c}} \quad (5-7)$$

Equation 5-7 can be used to determine the number of cycles to failure for a strain range $\Delta\varepsilon(i)$. The corresponding $2N_{f(i)}$ is used in Equations 5-4 and 5-5 to compute the damage index.

A total of four damage indices were computed for each random amplitude experiment:

- D_1 - a and c values were obtained from total strain range curve fit data. All constant amplitude experiments were considered.
- D_2 - Similar to D_1 except only the constant amplitude experiments involving the same bar size under consideration were used to determine a and c .
- D_3 - a and c values were obtained from plastic strain range curve fit data. All constant amplitude experiments were considered.
- D_4 - Similar to D_3 except only the constant amplitude experiments involving the same bar size under consideration were used to determine a and c .

For the damage indices involving plastic strain amplitude, the elastic portion of each deformation range must be removed. This is a very difficult quantity to determine due to the Bauschinger effect. After initial yielding of the specimen occurs, subsequent yield points are not well defined and vary with each cycle. Rather than determining the plastic strain ranges directly from the collected data, a linear relationship was obtained from the constant amplitude experiments that relates this quantity to total strain range:

$$\Delta\varepsilon_p = 0.833\Delta\varepsilon - 0.0023 \quad (5-8)$$

where: $\Delta\varepsilon_p$ = plastic strain range
 $\Delta\varepsilon$ = total strain range

Calculated damage indices are presented in Table 5-7. Even though an ideal value of one was not obtained for all cases, the computed damage indices do provide a good indication of when failure is likely to occur. There is also relatively close agreement between indices based on plastic and total strain amplitude. Additionally, the computed damage indices do not appear to be sensitive to a and c constants determined from each specific bar size. Utilizing curve-fit expressions from all constant amplitude experiments also provides similar results.

It is difficult to say with confidence why some of the specimens performed better than others. There is certainly enough scatter in the constant amplitude data to account for some error in the random strain history experiments. The sequence of applied deformation may also have an effect on the total fatigue-life, a factor not considered by Miner's damage index.

5.4 Cumulative Damage Approach

The damage indices computed in the previous section are very useful in making predictions regarding fatigue failure. However, this approach fails to address the ultimate effect of fatigue: a reduction in specimen ductility due to the repeated application of load or deformation. This concept is illustrated for a constant amplitude experiment in Figure 5-11. As soon as the tensile strain exceeds the maximum tensile strain limit, failure occurs. Assuming a linear relationship between the number of strain reversals and the maximum tensile strain limit, the following equation may be used:

$$\varepsilon_{mx} = \varepsilon_o - \frac{(\varepsilon_o - \Delta\varepsilon/2)}{2N_f}(HC) \quad (5-9)$$

where: ε_{mx} = maximum achievable tensile strain

ε_o = initial tensile strain capacity

HC = number of strain reversals experienced by specimen

This relationship can be further manipulated to determine the maximum achievable tensile strain after experiencing i strain reversals during a random amplitude experiment:

$$\varepsilon_{mx(i)} = \varepsilon_{mx(i-1)} - \frac{(a - \Delta\varepsilon_{(i)}/2)(2a)^{1/c}}{\Delta\varepsilon_{(i)}^{1/c}} \quad (5-10)$$

Table 5-7 Calculated Damage Indices for Random Amplitude Experiments

Experiment # (bar size)	Total Energy to Failure (MPa)	D ₁ (total strain, all specimens)	D ₂ (total strain, specific bar size)	D ₃ (plastic strain, all specimens)	D ₄ (plastic strain, specific bar size)
37 (#22)	452.8	0.669	0.651	0.650	0.635
38 (#22)	689.4	1.218	1.186	1.183	1.157
39(#22)	563.8	0.810	0.790	0.793	0.778
40(#22)	500.3	0.765	0.744	0.746	0.730
41(#22)	662.4	0.944	0.921	0.930	0.913
42(#22)	507.9	0.719	0.702	0.703	0.689
48(#25)	600	0.787	0.737	0.780	0.740
49(#25)	520.1	0.785	0.787	0.768	0.759
50(#25)	695.9	1.107	1.128	1.080	1.080
51(#25)	711.4	1.131	1.150	1.107	1.104
52(#25)	806.3	1.414	1.433	1.384	1.379
53(#25)	686.0	1.248	1.269	1.222	1.219
54(#25)	625.4	1.083	1.096	1.059	1.054
55(#25)	813.0	1.363	1.377	1.335	1.326
Average	631.05	1.003	0.998	0.981	0.969
Std. Deviation	108.1501	0.24233	0.257132	0.236666	0.241187

In this equation, ϵ_0 has been replaced with the experimentally determined constant, a . Suidan and Eubanks (1973) reported that this quantity is a reasonable approximation of the ultimate tensile strain. Mill report data also supports this assumption. Figure 5-12 provides the actual

strain history used in experiment number 41 along with the resulting maximum tensile strain as computed with equation 5-10. Failure of the specimen is predicted with reasonable accuracy by the damage model. Similar plots for all tests can be found in Brown (1996).

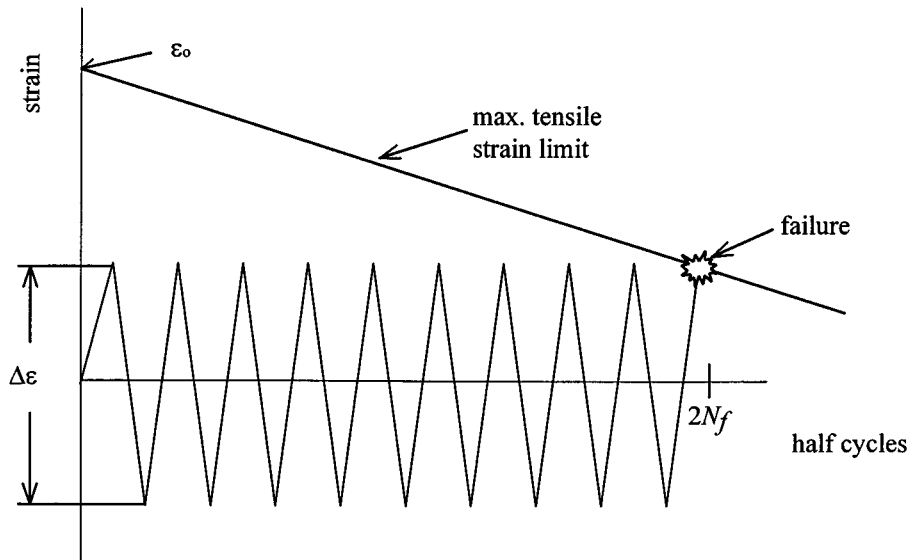


Figure 5-11 Cumulative Damage in Generic Constant Amplitude Experiment

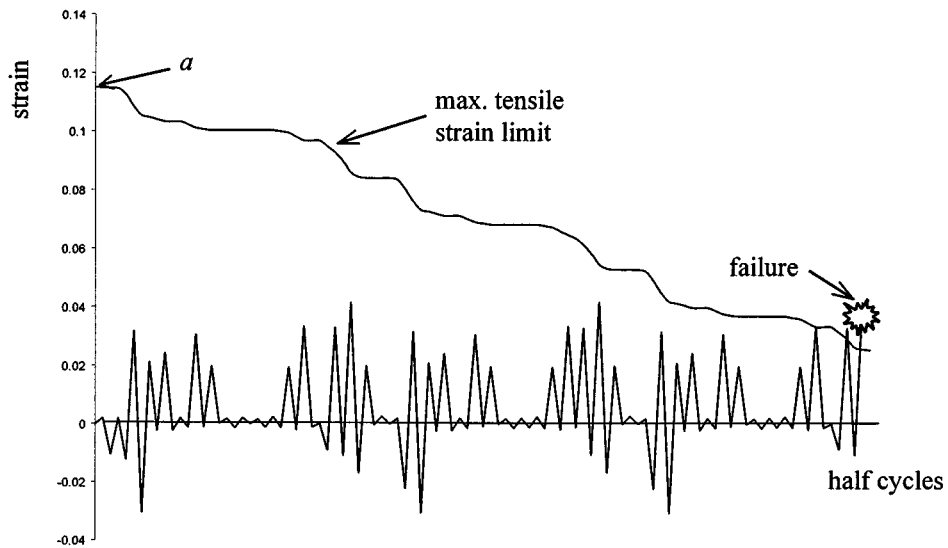


Figure 5-12 Cumulative Damage in Experiment #41

5.5 Application to Reinforced Concrete

It is important to realize that low-cycle fatigue failure of reinforcement is only one potential failure mode in a RC member. Though the damage model outlined in the previous section is capable of predicting failure in concrete reinforcement with some degree of accuracy, it does not address the effects of fatigue on confining steel or the performance of surrounding concrete. Such issues are beyond the scope of this research.

Rather than using this information to predict the exact point in a deformation history that a RC member is expected to fail, it is perhaps more logical to simply identify when low-cycle fatigue of reinforcement becomes a potential failure mode. Mander et al (1988) have shown that the ultimate strain achievable in well-confined concrete is near .05. It would be very unlikely that strains of any magnitude greater than this could be imposed on a member's reinforcement without also resulting in significant visible damage to surrounding concrete. Figure 5-1 illustrates this concept. As the maximum tensile strain limit drops below .05 (perhaps some other threshold value is more appropriate), low-cycle fatigue failure of reinforcement becomes a potential failure mode. Once this point is reached, the usable service life of a member has been spent and provisions for its retrofit or replacement should be considered.

Another observation made during these experiments that is also potentially relevant to RC was the inelastic buckling behavior exhibited by each specimen. Recall that considerable lateral bracing was employed in attempt to control this response with somewhat limited success. As mentioned previously, tension rupture of confining steel is a common failure mode in RC. The mechanism involved in this failure mode is not readily quantifiable in terms of plane section curvature and may in fact be heavily influenced by buckling of longitudinal reinforcement. Even at strains as low as .015, which far exceed the ultimate compressive strain of unconfined concrete, significant bar buckling was observed. Experimental results reported by Kunnath et al (1997) also support this observation in that all tension rupture failures of confining reinforcement were preceded by longitudinal bar buckling. This phenomenon may also have an adverse effect

on nearby concrete since any buckling between lateral reinforcement may also lead to a loss in confinement. Longitudinal bars, however, may buckle without rupturing the ties.

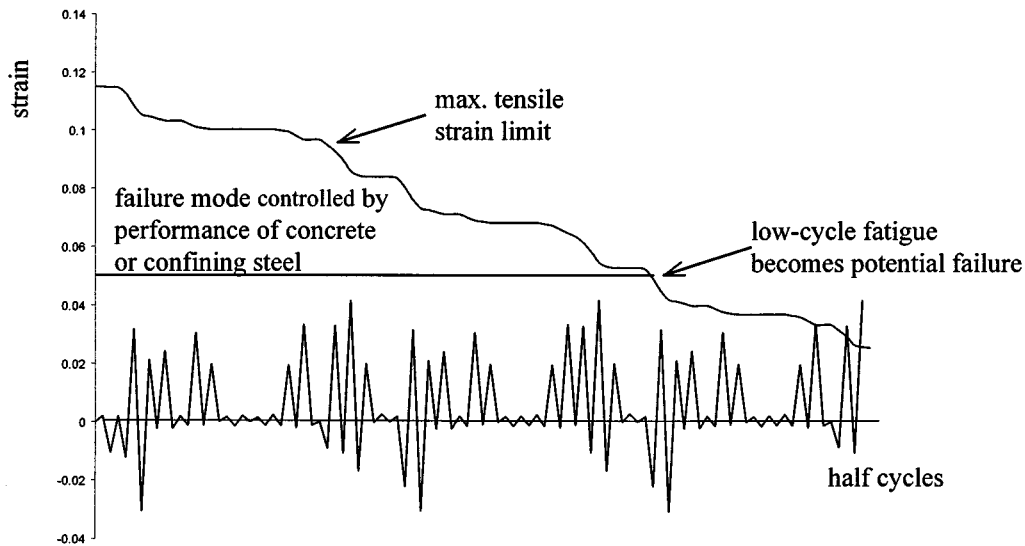


Figure 5-13. Damage Progression and Resulting Potential Failure Modes

5.6 Comparison With Previous Work (Mander et al, 1994)

The only other readily available information for comparison of results consists of a relatively small number of tests presented by Mander et al (1994) (specific details regarding these tests are presented in Section 1). Figure 5-14 provides the fatigue-life curves for total strain amplitude from Mander's 1994 study and the current study. The slopes of both curves are very similar; however, the current study results indicate consistently longer fatigue lives for the strain amplitudes under consideration. This is primarily due to the definition of fatigue life – which in Mander's study was defined as the appearance of the first fatigue crack while here it was considered at specimen failure.

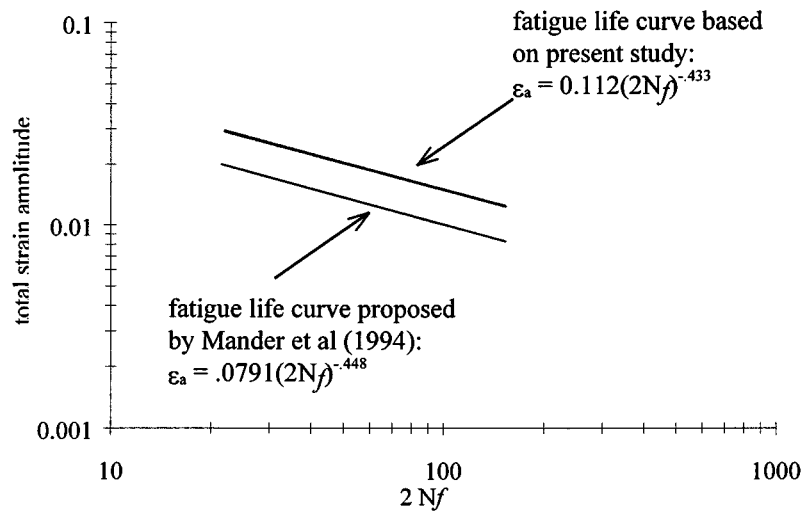


Figure 5-14 Comparison of Fatigue-life Curves: Current Study vs. Mander et al (1994)

Table 5-8 summarizes curve fit predictions from both studies. The following additional items have been identified as possible causes for differences in results:

- The deformation measurement technique employed in the present study results in a measure of average strain across the full gage length and not the peak strain experienced at the location of the fatigue crack. This would account for the resulting longer fatigue lives.
- The measurement technique employed by Mander does not accurately reflect specimen deformations due to inelastic buckling. Experiments performed in the current study with a similar technique did not yield consistent results.
- The specimen preparation process used in Mander's study involved welding. This may have resulted in the specimen test length being exposed to extremely high temperatures, thereby altering the fatigue-life of the material.

There are also several other variables that must be considered: different grades of concrete reinforcement were used, a different size of reinforcement was tested, and the rate of deformation differed by almost a factor of five. It must be noted, therefore, that since fatigue-life results are

extremely sensitive to experimental techniques, careful consideration must be used in their application to RC.

Table 5-8 Fatigue-life Summary (Curve Fit Predictions)

Total Strain Amplitude	Present Study Results ($2N_f$)	Mander et al (1994) ($2N_f$)
.015	104	41
.02	53	22
.025	32	13
.03	21	9

Note: $2N_f$ in Mander's tests were defined at the appearance of the first fatigue crack. In this study, it was defined at failure of the specimen.

5.7 Summary

The results of the fatigue testing presented in Section 4 were applied to numerous existing fatigue-life models. Fatigue life relationships for total strain amplitude and plastic strain amplitude were established. Correlation between total and plastic strain indices to the total strain energy was verified. Damage relationships were derived from the fatigue models developed for the constant-amplitude tests. The rainflow counting method was used to determine the number of cycles for the random amplitude tests.

The primary scope of this research is to contribute to current efforts in the development of performance-based criteria for the seismic design, retrofit, and repair of reinforced concrete bridge columns. It is the premise of the study that there exists an implicit relationship between seismic performance of a structural component, the imposed demand on the element and its capacity. The inter-relationship of these quantities can be derived through damage models. Consequently, the derivation of basic relationships to improve existing damage model

formulation so as to enable their use in practical design applications is also a significant objective of the study.

The following constitutes a brief summary of the essential findings of the research effort:

1. Bar size has a noticeable effect on fatigue life. Reinforcing bars with larger diameters exhibited improved fatigue characteristics.
2. Results of the testing indicate that definition of fatigue life is important when comparing different fatigue-life models. In this study, fatigue life was defined at the actual rupture of the rebar and not the first identification of a fatigue crack. In the present case it was found that the fatigue life expressions derived in this study varied significantly from those obtained by Mander et al. (1994) since the definition of fatigue life differed in the two studies. Additionally, the experimental setup, particularly the assembly and procedure used to grips the rebars, may have contributed to some of the observed differences.
3. Better correlations were obtained with damage models using total strain and plastic strain as opposed to energy-based formulations. The total energy dissipated to failure as a function of strain amplitude did reveal some trend, however, it was less reliable than measures utilizing strain-based parameters.
4. The rate of strength (stress) decay across tension peaks of the rebar can be an important precursor of failure. Strength loss beyond 75% of the original peak stress was rapid and catastrophic. The rate of decay for compression cycles was masked by local buckling phenomena.
5. The rainflow counting method was found to be satisfactory in dealing with random strain amplitudes, as would be expected in earthquake loading.

SECTION 6

REFERENCES

- Brown, J. (1996), "Fatigue Characteristics of Reinforcing Bars Under Simulated Seismic Loading." M.S. Thesis, Department of Civil and Environmental Engineering, University of Central Florida, Orlando.
- Cheng, Yi-Wen, and Broz, Jerry J., (1986), "Cycle Counting Methods for Fatigue Analysis with Random Load Histories: A FORTRAN User's Guide," Report No. NSBIR 86-3055, U.S. Department of Commerce, National Institute of Standards and Technology, Boulder, CO.
- Cheok, G.S., and Stone, W.C., (1986), "Behavior of 1/6 Scale Model Bridge Columns Subjected to Cyclic Inelastic Loading," Report No. NBSIR 86-3494, U.S. Department of Commerce, National Institute of Standards and Technology, Gaithersburg, MD.
- Coffin, L. F. Jr. (1954). "A study of the effect of cyclic thermal stresses on a ductile metal." *American Society of Mechanical Engineers*, 76, 931-950.
- Coffin, L.F., Jr., (1954), "A Study of the Effects of Cyclic Thermal Stresses on a Ductile Material," *Transactions of the American Society of Mechanical Engineers*, Vol. 76, pp. 931 - 950.
- Corley, W.G., Hanson, J.M., and Helgason, T., (1978), "Design of Reinforced Concrete for Fatigue," *Journal of the Structural Division, ASCE*, Vol. 104, No. ST6, pp. 921 - 932.
- Dutta, A. and Mander, J.B., (1998), "Capacity Design and Fatigue Analysis of Confined Concrete Columns," Report NCEER-98-0007, State University of New York at Buffalo, New York.
- Koh, S.K., and Stephens, R.I., (1991), "Mean Stress Effects on Low Cycle Fatigue for a High Strength Steel," *Fatigue Fracture of Engr. Materials and Structures*, Vol. 14, No. 4, pp. 413 - 428.
- Kratzig, W. B., and Meskouris, M. (1987). "Nonlinear seismic analysis of reinforced concrete frames." *Earthquake Prognostics*, Verlag Friedr, Vieweg and Sohn, Braunschweig, 453-462.

- Kunnath, S.K., El-Bahy, A., Taylor, A., and Stone, W.C., (1997), "Cumulative Seismic Damage of Reinforced Concrete Bridge Piers," Report NCEER-97-0006, State University of New York at Buffalo, New York.
- Kunnath, S.K., Reinhorn, A.M. and Lobo, R.F. (1992), "IDARC Version 3.0 – A Program for the Inelastic Damage Analysis of RC Structures." Report NCEER-92-0022, State University of New York at Buffalo, New York.
- Lorenzo, F., and Laird, C., (1984), "A New Approach to Predicting Fatigue Life Behavior Under the Action of Mean Stresses," *Materials Science and Engineering*, Vol. 62, No. 2, pp. 205 - 210.
- Lybas J. and Sozen M. A. (1977). "Effect of beam strength and stiffness on dynamic behavior of reinforced concrete coupled walls." *Report SRS Number 444*, Civil Engineering Studies, University of Illinois, Urbana, Ill.
- Mander, J.B., and Cheng, C.-T., (1995), "Renewable Hinge Detailing for Bridge Columns," National Seismic Conference on Bridges and Highways, San Diego, CA, December 10-13.
- Mander, J.B., Panthaki, F.D., and Kasalanti, A., (1994), "Low Cycle Fatigue Behavior of Reinforcing Steel," *Journal of Materials in Civil Engineering*, ASCE, Vol. 6, No. 4.
- Mander, J.B., Priestley, M.J.N., and Park, R., (1988), "Observed Stress Strain Behavior of Confined Concrete," *Journal of Structural Engineering*, ASCE, Vol. 114, No. 8, pp. 1827 - 1849.
- Manson, S. S. (1953). "Behavior of materials under conditions of thermal stress." *Heat Transfer Symposium*, University of Michigan Engineering Research Institute, Ann Arbor, Michigan.
- McCabe, S. L., and Hall, W. J. (1989). "Assessment of seismic structural damage." *Journal of Structural Engineering*, ASCE, 115, 2166-2183.
- Miner, M.A., (1945), "Cumulative Damage in Fatigue," *Journal of Applied Mechanics*, Vol. 12, pp. A-159.
- Park, Y., and Ang, A. H. (1985). "Mechanistic seismic damage model for reinforced concrete." *Journal of Structural Engineering*, ASCE, 111, 722-737.

- Park, Y.J., Reinhorn, A.M. and Kunnath, S.K. (1987). "IDARC: Inelastic Damage Analysis of Reinforced Concrete Frame Shear-Wall Structures." Report NCEER-87-0008, State University of New York at Buffalo, New York.
- Paulay, T., and Priestley, D. K. (1992). *Seismic design of reinforced concrete and masonry buildings*, John Wiley & Sons, Inc., New York, N.Y.
- Smith, W.F., (1990), "Principles of Materials Science and Engineering," McGraw-Hill, Inc., New York.
- Stone, W. C., and Cheok, G. S. (1989). "Inelastic behavior of full-scale bridge columns subjected to cyclic loading." *NIST Building Science Series 166*, National Institute of Science and Technology, Gaithersburg, Md.
- Suidan, Mubadda T., and Eubanks, Robert A., (1973), "Cumulative Fatigue Damage in Seismic Structures," *Journal of the Structural Division, ASCE*, Vol. 99, No. ST5, pp. 923 - 941.
- Wang, M., and Shah, S. P. (1987). "Reinforced concrete hysteresis model based on the damage concept." *Earthquake Engineering and Structural Dynamics*, 15, 993-1003.



MULTIDISCIPLINARY CENTER FOR EARTHQUAKE ENGINEERING RESEARCH

A National Center of Excellence in Advanced Technology Applications

University at Buffalo, State University of New York
Red Jacket Quadrangle ■ Buffalo, New York 14261-0025
Phone: 716/645-3391 ■ Fax: 716/645-3399
E-mail: mceer@acsu.buffalo.edu ■ WWW Site: <http://mceer.buffalo.edu>



University at Buffalo *The State University of New York*

ISSN 1520-295X